Copyright Warning & Restrictions

The copyright law of the United States (Title 17, United States Code) governs the making of photocopies or other reproductions of copyrighted material.

Under certain conditions specified in the law, libraries and archives are authorized to furnish a photocopy or other reproduction. One of these specified conditions is that the photocopy or reproduction is not to be "used for any purpose other than private study, scholarship, or research." If a, user makes a request for, or later uses, a photocopy or reproduction for purposes in excess of "fair use" that user may be liable for copyright infringement,

This institution reserves the right to refuse to accept a copying order if, in its judgment, fulfillment of the order would involve violation of copyright law.

Please Note: The author retains the copyright while the New Jersey Institute of Technology reserves the right to distribute this thesis or dissertation

Printing note: If you do not wish to print this page, then select "Pages from: first page # to: last page #" on the print dialog screen

ABSTRACT

SUBJECT AND GROUP LEVEL CHANGES AND COMPARISON IN FUNCTIONAL CONNECTIVITY UNDER LOW vs. HIGH COGNITIVELY DEMANDING NATURALISTIC VIEWING CONDITIONS USING fMRI.

by
Rakibul Hafiz

Resting State fMRI is used extensively for analysing brain regions. fMRI is also used to determine task induced activations from cerebral networks. This study involves both rest and task activation data and implements statistical methods applied on Blood Oxygenation Level Dependent (BOLD) signals. The conventional task based designs are very specific and may not reflect day to day activities. The two task conditions in this study are watching a movie called *INSCAPE* with low cognitive load and segments of contextual Hollywood movies under continuous and natural conditions.

The aim is to investigate individual and group level Functional Connectivity changes between REST and the two conditions - INSCAPE and MOVIE. The hypothesis is that the functional networks of INSCAPE emulate Resting State networks more closely than traditional MOVIES if the consistent group level effect is regressed out. Voxel wise regression is used on individual subjects across sessions and between subjects per session. Network Wise Correlation Coefficient Maps were also generated using Power's 264 ROIs. Group level concatenated (cICA), for all conditions, and tensor ICA (tICA) maps for only natural viewing conditions were also generated. A paired t-test was performed between INSCAPE vs. REST and MOVIE vs. REST conditions. The results show that ROIS with significant differences were considerably lower for INSCAPE than MOVIE for an FDR corrected arbitrary threshold of $p < 0.0005$.

SUBJECT AND GROUP LEVEL CHANGES AND COMPARISON IN FUNCTIONAL CONNECTIVITY UNDER LOW vs. HIGH COGNITIVELY DEMANDING NATURALISTIC VIEWING CONDITIONS USING fMRI.

by
Rakibul Hafiz

A Thesis
Submitted to the Faculty of
New Jersey Institute of Technology
in Partial Fulfillment of the Requirements for the Degree of
Master of Science in Biomedical Engineering

Department of Biomedical Engineering

August 2017

APPROVAL PAGE

SUBJECT AND GROUP LEVEL CHANGES AND COMPARISON IN FUNCTIONAL CONNECTIVITY UNDER LOW vs. HIGH COGNITIVELY DEMANDING NATURALISTIC VIEWING CONDITIONS USING fMRI.

Rakibul Hafiz

Dr. Bharat B. Biswal, Thesis Advisor — Date
Professor of Biomedical Engineering, NJIT

Dr. Sergei Adamovich, Committee Member — Date
Professor of Biomedical Engineering, NJIT

Dr. Xiaobo Li, Committee Member — Date
Associate Professor of Biomedical Engineering, NJIT

Dr. Xin Di, Committee Member — Date
Research Assistant Professor of Biomedical Engineering, NJIT

BIOGRAPHICAL SKETCH

Author: Rakibul Hafiz

Degree: Master of Science

Date: August 2017

Undergraduate and Graduate Education:

- Master of Science in Biomedical Engineering,
  New Jersey Institute of Technology, Newark, New Jersey, 2017

- Bachelor of Science in Electrical and Electronic Engineering,
  American International University-Bangladesh, Banani, Dhaka, Bangladesh, 2012.

Major: Biomedical Engineering

To my daughter… the Northern Star of my life and the fuel to my endeavors.

To my wife… the immovable rock of support and the love of my life.

To my parents… the reason for my existence and the epitome of compassion.

"To be nobody but yourself,

in a world which is doing its best, night and day,

to make you everybody else –

means to fight the hardest battle which any human can fight;

and never stop fighting."

– E. E. Cummings

ACKNOWLEDGMENT

I would like to express my sincerest gratitude to my advisor Dr. Bharat B. Biswal for his patience and support throughout the entire process of this project's completion. I would also like to thank and appreciate the committee members Dr. Sergei Adamovich and Dr. Xin Di for their insight and valuable advice on the project.

I would like to thank Dr. Max Roman, the academic coordinator of the Masters Program in the BME department for his relentless help and support. I am very grateful to every lab member at the NJIT Brain Connectivity Lab for being so patient and kind on me. I express my earnest gratitude to Suril for teaching me so much in such a short time. I must mention Rui and Keerthana for their solidarity in suggestions and mentorship in Suril's absence. I am glad I was able to work with such a hard working team.

TABLE OF CONTENTS

TABLE OF CONTENTS
(Continued)

TABLE OF CONTENTS
(Continued)

Chapter **Page**

TABLE OF CONTENTS
(Continued)

Chapter **Page**

LIST OF TABLES

LIST OF FIGURES

LIST OF FIGURES
(Continued)

Figure **Page**

CHAPTER 1

INTRODUCTION

1.1 Naturalistic Viewing Paradigm

This study focuses on functional connectivity changes in an adult population using a naturalistic viewing paradigm. Traditional task based studies follow a specific block design set by the experimenter. However, naturalistic viewing paradigms such as watching videos and movies or listening to music, comprise of stimuli that are continuous and dynamic. They do not follow any specific block design. Thus, the stimulus presented to the subjects would reflect natural day to day activities.

Two categories of movies representing naturalistic viewing paradigm are presented in this study. The first movie stimulus is called INSCAPE which consists of abstract 3D shapes, with no verbal and social context (Vanderwal et al., 2015).The first stimulus had three versions. The second stimulus contains segments from three typical Hollywood movies. The first three sessions presented a different version of INSCAPE and MOVIE. Then, they would be presented in a different order because each subject would undergo twelve sessions.

Vanderwal et al. used two categories of movies to improve head motion compliance in children and adults. They used frame-wise displacement (FD) to quantify the head motion and conventional movies achieved highest head motion compliance retaining about 79% of usable data with INSCAPES coming close to a 77% compared to only 44% in Resting State (Vanderwal et al., 2015). Their study also showed fewer number of sleep induced subjects during the movie tasks compared to resting state. Since

INSCAPE has very low cognitive demand, it was suggested as a possible intermediate stage between REST and high cognitive demand Hollywood movies. This is because INSCAPE's low cognitive demand makes it a task state closely emulating resting state, while providing better head motion compliance, specifically in children. This allows a clinical advantage to scan children population.

1.2 Introduction to fMRI

fMRI is a scanning technique used to acquire images non-invasively. It presents information based on cerebral blood flow and metabolic processes. PET had been used earlier to look into the cognitive aspects of the brain (Posner et al., 1988). It uses radioactive tracers to measure metabolism or glucose consumption. However PET's availability was limited. Eventually, functional Magnetic Resonance Imaging (fMRI) became preferable because it is non-invasive and can be easily incorporated into already established MRI machines. It is an indirect approach to determine the functionally connected regions of the brain using Blood Oxygenation Level Dependent (BOLD) responses. The details of fMRI and its advantages over other paradigms will be discussed in Chapter 2.

The initial fMRI studies were task based. There is temporal coherence in Brain Networks related by BOLD responses corresponding to task based activities (Fransson et al., 2006, Calhoun et al., 2008). Studies on resting state conditions also began using fMRI. The first demonstration of using fMRI to analyse and define large spatially and functionally connected networks in the brain under resting state conditions was shown by Biswal et al. in 1995. It has been used to study patients who are neurologically or

physiologically challenged to perform a regular task. For example, it has been used to study Alzeihmer's patients and healthy controls (Li et al., 2002, Greicius et al., 2008).

1.3 Objectives

The first objective was to investigate spatial patterns across three conditions and temporal consistency in task conditions. Concatenated ICA (cICA) was performed on all conditions to compare independent connectivity maps within and across conditions. Tensor ICA (tICA) was performed on each task condition to derive networks showing activation due to consistent task effect.

The second objective of this study was to verify if functional connectivity during INSCAPE viewing approaches the REST condition after consistent task effect is removed from individual subjects. Individual and group level changes in functional connectivity in adults aged between 21-42 years old during INSCAPE and MOVIE conditions are compared with the REST condition. A paired *t*-test with FDR (False Discovery Rate) correction was performed to observe for significant differences across conditions.

1.4 Future Implications

The study shows significant connectivity differences in ROIs are comparatively lower for INSCAPE (< 50%) than the traditional MOVIE condition. Statistical analysis demonstrates ROIs from major networks contributing activations during INSCAPE and MOVIE viewing. Middle Occipital and Inferior Occipital gyri from the visual network indicate significant differences. Left Precentral gyrus from Cingulo Opercular Network, Cingulate and Middle Frontal Gyri from Default Mode Network demonstrate significant

differences during INSCAPE. ROIs from attention, visual, auditory, salience and subcortical networks show significant differences during MOVIE. Superior Temporal Gyrus from ventral attention network, Middle Temporal Gyrus from dorsal attention network, Medial Frontal Gyrus from cingulo opercular network and Inferior Frontal Gyrus from salience network including more than seventy other ROIs show significant differences during MOVIE viewing. Number of ROIs with significant differences is almost double than the corresponding INSCAPE condition.

In the future, the analysis presented here could be extended on a children group to investigate if they respond to these stimuli differently. Differences in connectivity could be compared between REST, INSCAPE and MOVIE to see if any of these conditions has a greater effect on a specific age population. Sensitivity of children to a specific genre of movies could also be investigated. For example, Vanderwal et al. used *'Fantasia'* for children and *'Ocean's Eleven'* for adults. The two age populations can respond differently to two different movie stimuli. An experiment can be set up to investigate changes in functional connectivity, while both sample groups commonly view one movie appropriate for both age groups between teenagers and adults.

Regression of task selective dynamic properties that moderate the functional connectivity could be another plausible approach to get INSCAPE connectivity similar to REST connectivity. Two alternative approaches could also be implemented. Firstly, instead of regressing out the effect of all subjects only half of the sample population is randomly selected and their consistent effect is regressed out. Secondly, the first two Principal Components derived from the time-series of an entire group'stask effect is regressed out. A non-parametric approach with controlled FPR (False Positive Rate)

based on the work of Chen et al. could also be implemented to compare the functional connectivity derived from parametric tests. A more rigid statistical approach could be applied in the future. This would require a one sample *t* – test on each session's dataset and then apply a post hoc analysis on selective ROIs with significance from the first stage.

1.5 Outline

This thesis has six chapters. Chapter 1 introduces the thesis topics and the naturalistic viewing paradigm. It also points out the objectives and future implications of this study. Chapter 2 is a brief introduction to the basics of MRI scanning techniques and data acquisition methods for this study. Chapter 3 provides details of the image processing steps and statistical analysis performed. Chapter 4 describes the three different methods applied to estimate the functional connectivity of REST, INSCAPES and MOVIE dataset. Chapter 5 shows all the results with corresponding figures. Chapter 6 ends this thesis with conclusion and discussion of the results from Chapter 5.

CHAPTER 2

MRI SCANNING AND DATA ACQUISITION

2.1 MRI Scanning Techniques

This study was performed on a dataset that is publicly available online (http://fcon_1000.projects.nitrc.org/indi/hbn_ssi/download.html). MRI and fMRI imaging techniques were used for obtaining anatomical and functional information in the form of 3D and 4D datasets respectively.

2.1.1 MRI Review

A brief overview of the MRI instrumentation is introduced in this section. An MRI machine consists of powerful magnets having high magnetic field strengths starting from 1.5T (Tesla) to 3T, 7T or even 14T. High field MRI is used to study animals. The MRI scanner consists of three major components - the main magnet, the gradient coil and the RF system.

The main magnet is a large electromagnet that produces the main magnetic field. It is denoted by $\boldsymbol{B_0}$. The Gradient coils are implemented for spatial encoding or localization of the MR signal (Hidalgo-Tabon et al., 2010). Shim coils are used to correct for inhomogeneities in the magnets and make sure the main magnetic field $\boldsymbol{B_0}$ is as homogeneous as possible (Jerrord et al., 2012). The RF (Radio Frequency) coils are used to give rise to the radio frequency field $\boldsymbol{B_1}$ which changes the direction of $\boldsymbol{M}$, the net magnetization**.** $\boldsymbol{M}$ consists of two time dependent parts: longitudinal Magnetization $\boldsymbol{M_z}$ and transverse magnetization $\boldsymbol{M_{xy}}$. It is an average measure of the angular momentum of the nuclear spins away from $\boldsymbol{B_0}$. These coils excite and moderate the nuclear spins in the

subject and they are also responsible in the detection of the response signals (Klomp et al., 2011.). They typically act both as a transmitters and receivers.

2.1.2 Flip Angle, T1 and T2 Relaxation

Flip Angle

Flip Angle is a quantitative measure of the amount by which the $\boldsymbol{B_1}$ field rotates the longitudinal magnetization, $\boldsymbol{M_z}$, while being applied at an orthogonal plane with respect to the $\boldsymbol{M_z}$ vector (Jerrord et al., 2012). Very well known flip angles used currently are 90 degrees and 180 degrees with a wide range of other smaller and larger angles implemented for different scanning techniques requiring specific anatomical feature display. It can be calculated from the equation:

$$\boldsymbol{\theta = \omega_1 t} \tag{2.1}$$

$\boldsymbol{\theta}$,is the flip angle. $\boldsymbol{\omega_1}$ is the angular frequency, which represents the rate at which the $\boldsymbol{M_z}$ is rotating in the transverse plane. $\boldsymbol{\omega_1}$ is governed by the Larmor equation:

$$\boldsymbol{\omega_1 = \gamma B_1} \tag{2.2}$$

$\boldsymbol{\gamma}$ is the gyromagnetic ratio. This constant is dependent on nuclear specificity. $\boldsymbol{B_1}$ is the applied 90 degree radio frequency pulse over the period $\boldsymbol{t}$. The flip angle equation can be expanded by replacing $\boldsymbol{\omega_1}$(Jerrord et al., 2012):

$$\boldsymbol{\theta = \gamma B_1 t} \tag{2.3}$$

T1 Relaxation

The T1 relaxation is a process in which the longitudinal magnetization, M_z recover back to the equilibrium condition. This is also known as spin-lattice relaxation time. The relaxation time relies on the rate at which the energy is being dissipated to the surrounding tissue types (Jerrord et al., 2012).

This can be represented by the following equation:

$$\boldsymbol{M_z(t) = M_0(1 - e^{-t/T1})} \tag{2.4}$$

where $\boldsymbol{M_z(t)}$ is the instantaneous longitudinal magnetization at time $\boldsymbol{t}$, $\boldsymbol{M_0}$ is the equilibrium longitudinal magnetization and $\boldsymbol{T1}$ is the time required for $\boldsymbol{M_z(t)}$ to recover 63% of $\boldsymbol{M_0}$ after a 90-degree pulse.

T2 Relaxation

The T2 relaxation is the process by which the transverse magnetization $\boldsymbol{M_{xy}}$ decays exponentially to 37% of its peak value that was present at the beginning of the transverse magnetization after a 90 degree pulse was applied (Jerrord et al., 2012). The time taken for this process to complete is the T2 relaxation time. This can be represented by the following equation:

$$\boldsymbol{M_{xy}(t) = M_0 e^{-t/T2}} \tag{2.5}$$

where $M_{xy}(t)$ is the instantaneous transverse magnetization at time t, M_0 is the initial maximum transverse magnetization and $T2$ is the time required for $M_{xy}(t)$ to decay to 37% of M_0. Any specimen that drives T1 relaxation also causes T2 relaxation however T2 relaxation can also occur independently without any occurrence of T1 relaxation (Bloch, 1946). The loss of coherence in the transverse magnetization, M_{xy} gives rise to free induction decay (FID) signal which appears to be a damped sinusoidal signal.

2.1.3 TR and TE

TR

A complete session of MR imaging depends on many cycles of repetitive pulse sequences to accumulate enough data to create an entire dataset. The timing of these pulse repetition sequences determines different scanning techniques. Time of Repetition (TR) is defined as the interval of time between B_1 excitation pulses. In one TR interval a **T2** decay and a **T1** relaxation occur (Jerrord et al., 2012). Usually pulse sequences would consist of several of these TR intervals with different values to generate different types of MR images.

TE

A 90 degree B_1 pulse, also known as excitation pulse, is usually shortly accompanied by a 180 degree RF inversion pulse. As a result, it induces an echo to avoid mixing the energy dissipation and incoming response signal. The Time of Echo (TE) is simply the interval of time between the excitation pulse and the peak of the induced echo (Jerrord et al., 2012).

2.2 T1 MP-RAGE Images

The anatomical scan, mentioned in the early part of section 2.1 in this chapter, is also referred to as an MP-RAGE or a T1 Weighted image. MP-RAGE stands for Magnetization Prepared Rapid Acquisition GRE where GRE further expands into Gradient Recalled Echo. Basically, this scanning technique generates a 3D volume with very high spatial resolution and fine slices. T1 images usually have relatively short TR and TE (Jerrord et al., 2012). It provides distinct contrast differences between different tissue types in the brain and tissues like grey matter, white matter, Cerebrospinal Fluid (CSF) and the ventricles are very easily distinguishable in this kind of image.

Figure 2.1 shows a T1 image of a subject from the current study, in all three orthogonal (Axial, Sagittal and Coronal) planes. All three images are from the same subject at a particular slice from its brain. The different tissue types are clearly identifiable in this T1 image.

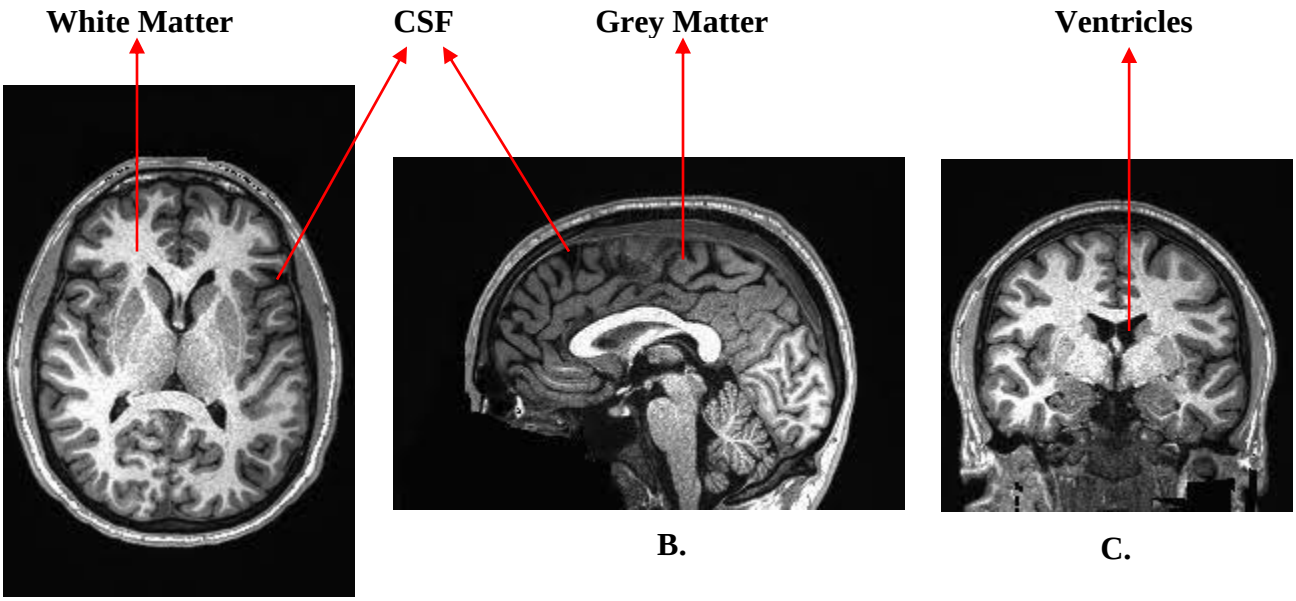

Figure 2.1 A T1 MP-RAGE image of an anonymous subject from the current study. **A**. Axial View; **B.** Sagittal View; **C.** Coronal View with different tissue types labeled.

Source: http://fcon_1000.projects.nitrc.org/indi/hbn_ssi/download.html, Raw Data Accessed on Dec 15, 2016.

2.3 Functional Magnetic Resonance Imaging (fMRI)

The functional images carry temporal information. Multiple shots of images are taken across constant TRs, over a period of time. This allows detection of any changes in activations per unit time over specific ROIs for a task or over the entire brain networks like in resting state conditions.

The general MRI or T1 images represent information based on the magnetic property of the hydrogen nuclei in water molecules of the subject. The fMRI BOLD signals represent information based on the amount of oxygen consumption, blood flow and blood volume in the target neurons. The first novel experiment to establish the link between cerebral blood flow and human brain functionality was performed by Angelo Mosso in 1884 (Stefano et al., 2013). The design of this experiment was based on

implementing a delicate balance with the subject lying horizontally on top. The table would tip towards the side with the subject's head due to blood flow to the cerebral cortex while the subject performed a cognitive task. It would also cause a marker on the opposite end to go up and down and generate a response signal. The task for the subject was to do intellectual mathematical calculations in his head while data was simultaneously recorded.

Active neurons use more energy and consequently require more oxygen. This creates a higher demand for oxygenated blood. Eventually vasodilation occurs in the surrounding blood vessels causing more blood with oxygenated blood to flow. Therefore, when a brain region is active, blood flow and the amount of glucose breakdown increases at a higher level than oxygen consumption.

The loss of oxygen from hemoglobin in blood creates deoxygenated blood. Deoxygenation in blood vessels changes the magnetic susceptibility of the water protons (Ogawa et al., 1990). This loss of oxygen from the hemoglobin molecule changes the magnetic properties of the blood proportionally. As the deoxy-hemoglobin molecules bind with more oxygen, the homogeneity of magnetic susceptibility increases. So, when the oxygenated blood increases locally more than the oxygen consumption, the BOLD signal gets enhanced and vice-versa. Essentially, fMRI is an indirect measure of neuronal response determined from the level of metabolism involved. The studies built on fMRI depend on the modulation of BOLD signals.

Figure 2.2 shows a typical fMRI image with a BOLD signal also shown at the top from a particular voxel. Compared to T1 images, the low spatial resolution of functional images is quite evident.

2.3.1 Blood Oxygen Level Dependent (BOLD) Signals

Ogawa et al. demonstrated that deoxygenated blood acts as a natural contrast agent under gradient echo imaging using MRI which consequently generated the concept of BOLD signals (Ogawa et al., 1990). The onset of any stimulus in a neuron leading to a response happens faster than the BOLD response. To state simply, the physiological changes such as blood flow and oxygen consumption are much slower than neuronal responses. A Hemodynamic Response Function (HRF) signal is approximately similar to the neuronal response. It is a noiseless response to a very short stimulus (Poldrack et al., 2011).

HRF and BOLD signals can be approximated to Linear Time Invariant (LTI) signal characteristics (Cohen, 1997; Boynton et al., 1996; Dale, 1999). This means BOLD signals get modified linearly with neuronal responses and also follow the same time shift in signals with respect to the stimuli. To achieve accurate BOLD signals for a given stimulus, a convolution is done between the HRF signal and the time series of the stimulus signal. Studies show the use of double gamma HRF to account for poststimulus undershoots (PSU) and derivatives generating a number of basis functions to correctly estimate the shape of the hrf signal owing to its variability across subjects (Friston et al., 1998, Glover et al., 1999).

Resting state spontaneous BOLD signal activity exhibit slow frequency fluctuations (< 0.1 Hz) while its faster frequency components relate to physiological phenomena such as breathing and cardiac cycles (Biswal et al., 1995, Cordes et al., 2001). For most task based experiments these signals would be considered as noise and averaged out (Fox et al., 2007). But it was shown that the somatomotor and medial motor regions produce such fluctuations even when there was no motor task involved (Biswal et

al. 1995). The challenge was to isolate these 'non-noise' BOLD signals from other artifacts. Several methods have been introduced to derive these independent BOLD signals in resting state situations.

One way to isolate the low frequency signals from the high frequency cardiac and respiratory signals is to measure the physiological parameters and apply them in a linear regression model to get rid of the noise (Birn et al., 2006). A data driven approach that is frequently used is an Independent Component Analysis (ICA) to estimate independent BOLD signals as independent components (Beckmann, et al, 2005). This method also isolates the noise signals as separate components. Another method used to reduce physiological artifacts is regression of signals from regions such as white matter, CSF and the ventricles (Fox et al., 2005) because these regions generate high artifact signals. Similar methods were also used to reduce noise from the BOLD signals of the dataset involved in the current study. They will be discussed in Chapter 3.

2.3.2 Advantages Over Other Paradigms

fMRI is non-invasive. Chapter 1 mentioned briefly about harmful effects of ionizing radiation associated with X-ray, CT and PET. fMRI technology is independent of such harmful radiations so it can be used for scanning subjects of various ages. fMRI has been used on healthy children and adults for the same study (Vanderwal et al., 2015). fMRI is much faster than PET. PET scans require at least one minute (Poldrack RA et al., 2011) for one particular task. On the other hand, high scanning rate of fMRI can be used to study event-related (ER) designs involving short-lived stimuli. fMRI has been reported to act as a biomarker (Glover GH, 2011). It has been used a biomarker for a multi-site Schizophrenia study (Kim DI, 2010).

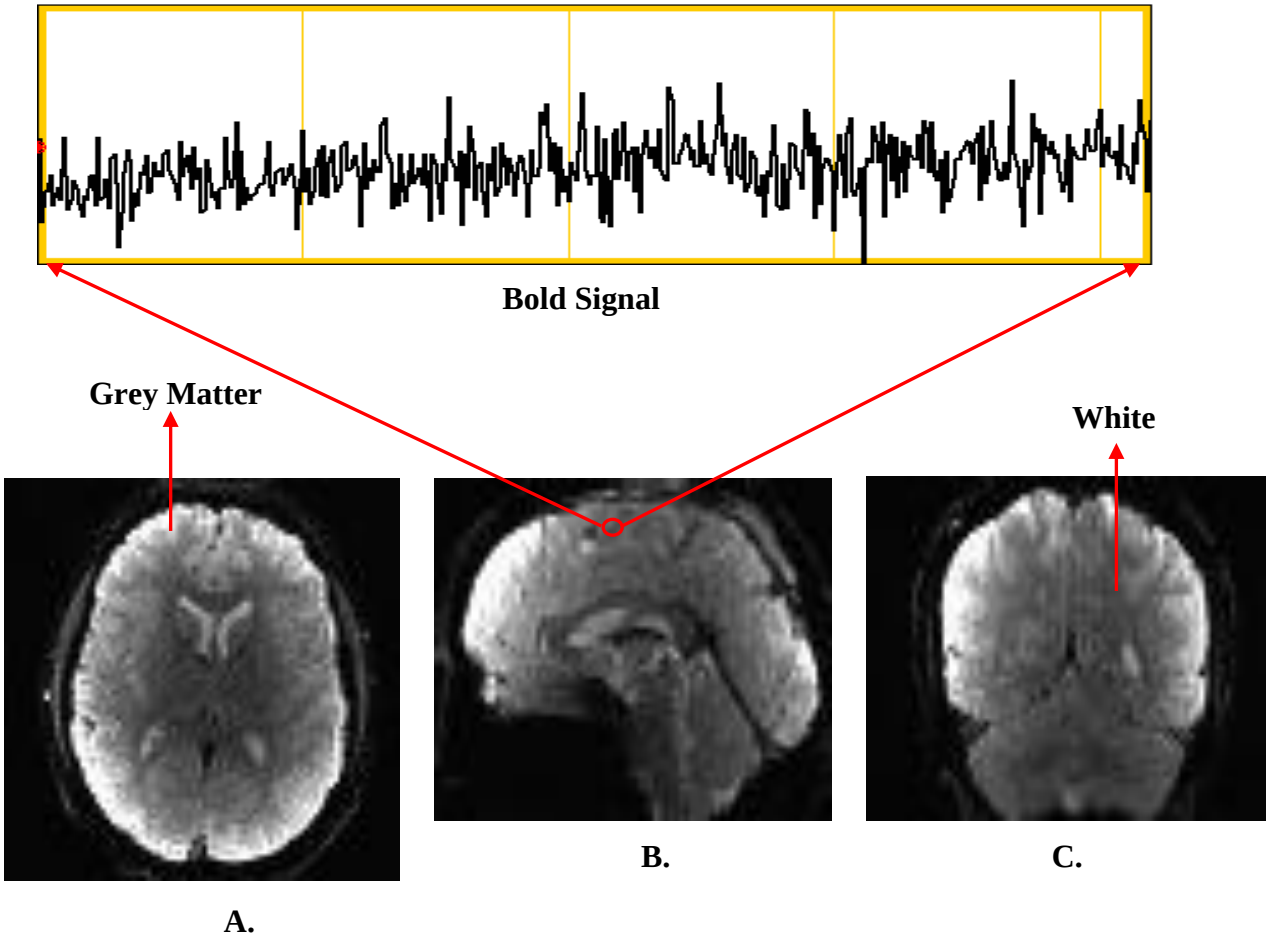

Figure 2.2 An fMRI image of an anonymous subject from the current study. **A**. Axial View; **B.** Sagittal View; **C.** Coronal View. A BOLD response is shown to be zoomed in from an arbitrary position of the Sagittal slice (**B**). The white matter appears darker and the grey matter appears brighter in fMRI images. Compared to **Figure 2.1** the spatial resolution of fMRI images is quite low.

Source: http://fcon_1000.projects.nitrc.org/indi/hbn_ssi/download.html, Raw Data Accessed on Dec 15, 2016

fMRI is easily compatible with regular MRI machines which are used abundantly for clinical diagnosis. Although fMRI lacks in spatial resolution compared to T1 MRI images, it has high temporal resolution. Yet, the spatial resolution of fMRI is superior to PET images. It is possible to use fMRI images for simple image subtraction between 'task-on' vs 'task-off' conditions to generate activation maps (Kwong, KK, et al., 1992).

2.3.3 Limitations of fMRI

The high speed scanning in fMRI requires bigger pixel sizes to sustain optimum Signal to Noise Ratio (SNR). This causes a loss in spatial resolution. Usual fMRI image resolution is 3-4 mm compared to 1 mm resolution of T1 images. Yet fMRI has relatively higher resolution than its contemporaries such as PET (5-10 mm) and NIRS (10-20 mm). The temporal resolution of fMRI is limited by the timing of the BOLD response. This is due to the time difference between BOLD signal generation and actual neural responses that was mentioned in Section 2.3.1. But this issue is addressed using corrective methods. A study mentions about the spatial distortion in fMRI in the frontal orbital and lateral parietal regions (Cho ZH, 1992). This arises from the magnetic susceptibility differences in the air-brain interface. fMRI is prone to motion artifacts. There are numerous methods applied to get rid of these motion generated noise from the BOLD signals. Acoustics can become a factor due to the repetitive deafening sound during fMRI scanning. Usually subjects are provided with air-plugs or noise cancelling headphones to avoid damage to their ears and prevent any unwanted signals as noise. It is not a viable paradigm for claustrophobic patients so usually a precautionary questionnaire is prepared for the subject before the scanning session. fMRI or regular MRI can not be used on a patient who has metal implants or tattoos since this will not only distort the image with artifacts but also can cause severe physical damage to the subject.

2.4 Inscapes and Movie

Inscapes

INSCAPES were briefly introduced in Chapter 1. This movie was used for better head motion compliance in children and clinical populations during fMRI (Vanderwal et al., 2015). But regular movies have shown maximum reduction in head motion. However, INSCAPES are not used just for better head motion compliance. The aim of Vanderwal et al. was to use it as a mediatory mode between Resting State and a heavily cognitive task like watching Hollywood movies. In essence, the suggestion was to use it an intermediate stage which resemble Resting State conditions where the subjects typically get drowsy and make a lot of head motion. But to get close to Resting State Conditions INSCAPES had to be made with no social content. It has no language so as to activate the language processing areas of the brain. It has no cuts or sudden changes in frames or context like traditional movies which usually demands cognitive attention. It is basically a movie with evolving 3D abstract geometrical shapes. It is a computer generated animation created by a visual artist named Tobias S. Hoffmann. He made three versions of INSCAPES which were used in the current study for different scanning sessions. Limited color changes were used and the luminance was normalized. It runs at 25 frames per second and has a resolution of 1024 x 800 pixels. The audio used for the movie is a piano score that was created by Jodi S. Vander Woude. It is a stereophonic score sampled at 48 KHz and it was designed to mould the noise associated with Echo Planar Imaging (EPI) with the musical score. The music is based on the pentatonic scale which is a common structure for majority of listeners around the World. It is an open access material that can be found at: **headspacestudios.org/inscapes**.

Movie

Several movie clips were used in this study. They ranged from Hollywood live action to animation movies. These movies contained high 'cognitively' demanding contents. That is where the general movie watching task differed with INSCAPES. The sequence of tasks was counterbalanced in this study and different sessions had different order of tasks. The sequences will be discussed in Section 2.6. Clips of approximately ten minutes were used from three different movies as stimuli. The clips were taken from the following movies: Wall E, The Matrix and A Few Good Men.

2.5 Participants

Thirteen healthy, right-handed adults between 21 – 42 years of age (Mean Age: 30.45 years and Std. Dev: 6.16 years) were selected for this study. There were 7 females and 6 males in this study. However due to scanning and segmentation issues one of the subject's data was discarded for the current study, giving a sample size of n=12 and a 1:1 Male to Female ratio. Since this study was done on a data that was already acquired the full disclosure to the experimental procedure and set up is not possible here. However, all phenotypic and experimental information is provided in the source website mentioned in Figure 2.3 where the raw data were collected from.

2.6 Acquisition Methods

The team, who performed the scanning, also added an additional task besides REST, INSCAPES and MOVIE. The subjects also had to do a FLANKER task. They utilized three different FLANKER sequences across different sessions. However, in the current study only the REST, INSCAPES and MOVIE tasks were given preference. The original

task sequence is presented here with the FLANKER task. The twelve subjects mentioned in Section 2.5 had to undergo twelve sessions of scanning. Each session had a different sequence of tasks while the content of the individual tasks remained the same across sessions.

Figure 2.3 is a schematic outline of three such sequences used for one subject across three different sessions. This subject went through nine more sessions each with a different sequence of tasks. All the other subjects had similar sequences of tasks in different sessions respectively. The duration of each task was 10 minutes and the associated TR was 1450 milliseconds (ms) or 1.45 seconds. So including some extra scans, each condition would have 420 time points or functional images.

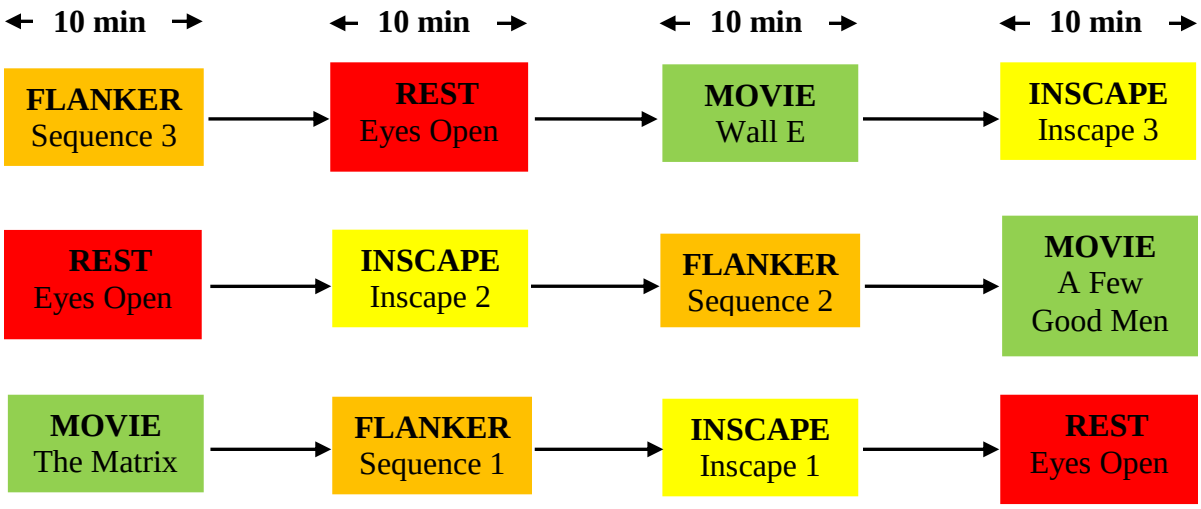

Figure 2.3 A schematic diagram of the task sequences applied on an anonymous subject from the current study. Sequences were picked from three different sessions. Each row of boxes represents task stimuli from one particular session for a particular subject. Each subject had to undergo 12 separate sessions with each session having a different sequence of these four tasks.

Source: http://fcon_1000.projects.nitrc.org/indi/hbn_ssi/download.html, Raw Data Accessed on Dec 15, 2016)

CHAPTER 3

IMAGE PROCESSING METHODS

fMRI studies require some image and signal processing before statistical analysis are implemented on the dataset. It starts from reconstructing raw DICOM images into NIFTI or other preferred formats after which, a series of analysis methods are applied. The same pre-processing methods were applied to each session and the set of twelve subjects on repeat. Scripts were written for each step and then run in a batch from the Statistical Parametric Mapping software SPM12 in MATLAB (MathWorks, Natick, MA). Both AFNI (Cox, 1996) and MATLAB were used for both pre-processing and analysis stages. However AFNI was mainly used in the primary stages to create masks and make physical changes such as adjusting field of view to the images. After those modifications, subject level brain recentering, the entire pre-processing and analysis were done on SPM12, exclusively for the pre-processing part. Once the images were transferred to standard space, occasionally AFNI was revisited for specific pre-analysis preparations. Images are basically two dimensional or three dimensional matrices with pixel intensities as their elements.

3.1 Pre-Processing

This is the primary stage before analysis is performed. Pre-processing is applied to make sure the data is properly oriented, have reduced motion artifacts, normalized and ready to go for any statistical analysis. It is a means to achieve statistically significant results because all other chances of an outlier have been taken care of. It is a process to make

sure that only the confounding variable is causing the statistical significance and not a systemic or instrumental artifact. The next sub-sections discuss the pre-processing steps used in this study.

3.1.1 Realignment

This process is mainly applied to the functional images. It is very likely that while scanning is in progress the subject would move and they do move. Consequently, some of the images in a time-series will not have proper alignment to a reference image, which could be the first, third or the mean image. It is important that all the images are aligned as a collection because even a slight movement in physical space could change pixel intensity significantly to cause an error in the final results (Friston et al., 1996). It uses a least squares method with a six parameter rigid body transformation (Friston et al., 1995). These are also known as the six motion parameters. They represent three translations in x, y and z axes and three rotations in roll, pitch and yaw. SPM produces an output file with information on these six parameters which are later applied on a regression model to get rid of any motion related artifacts.

3.1.2 Coregistration

Spatial Coregistration of functional images in SPM comes with three options – Coregister: Estimate, Reslice and Estimate and Reslice. Mostly the Coregister Estimate option is used and the images are not resliced. That is mainly because the images will undergo deformation or normalization to a standard space and they will eventually be resliced after that step. However, Estimate and Reslice is also used when normalization becomes an issue like if the images are not to be transferred to a standard space. If

Coregistration fails, then all the subsequent steps will produce erroneous results. What this step does is either register the functional images to the anatomical image of the same subject or vice versa. The former registration method is often used before the functional images are finally transferred to a high resolution anatomical standard space. Once the registration estimate is complete, the voxel-for-voxel affine transformation matrix and the histograms prior and post registration are presented in an output figure window with the registered images at the bottom. The original histogram usually lies on upper left side of the figure while the final joint histogram lies on the upper right (see Figure 3.1). The anatomical or the reference image with all three orthogonal planes are displayed at the bottom left while the functional or source files are displayed at the bottom right portion of the figure. The registration parameters are stored as header file information on the images undergoing coregistration.

The options for this step include a ‘reference’ image which is the image that remains stationary and if the functional images are being coregistered to the anatomical, then the anatomical image will be the reference image. The ‘source’ and ‘other’ images are the functional images that will undergo the affine registration processes, in other words, translated and rotated to match the reference image. There are also other options which are usually kept at their default values unless otherwise required for manual override.

Figure 3.1 is a sample figure generated from the coregistration of a single subject from a single session of the current study’s dataset. It is being presented here in order to show what the output figure of a Coregistration step looks like. If the registration was done properly, then the spatial positions on the low resolution functional images should

coincide with the high resolution spatial positions of the anatomical image. The bottom section of Figure 3.1 shows that the functional images (RIGHT) of Subject01 resting state condition from Session1 do have very good registration with the same subject's anatomical T1 image (LEFT). It should be noted that the source image, i.e., the REST image file has a prefix of 'r', which means the output file of the Realignment stage is being input here for the Coregistration step.

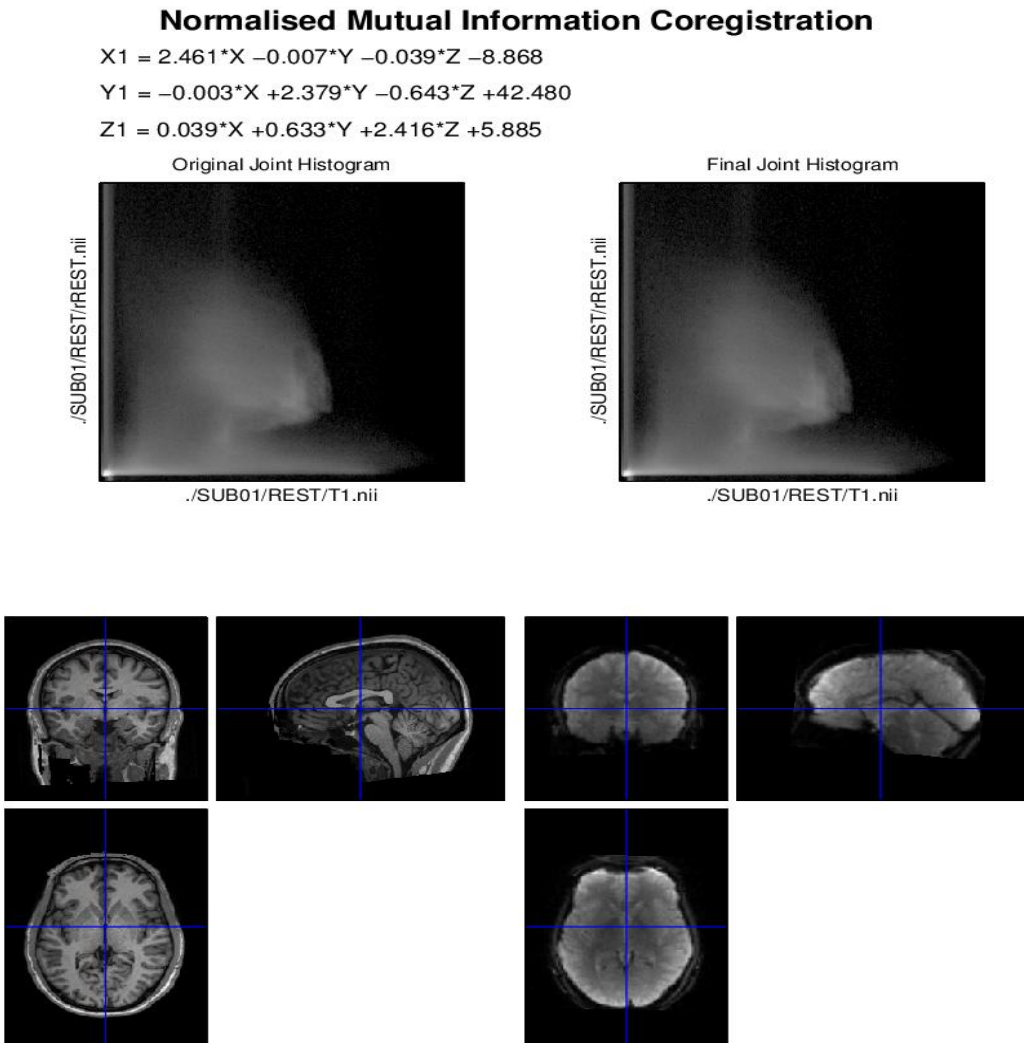

Figure 3.1 A single session, single subject output figure of coregistration generated as a sample for visualization purposes.

Source: http://fcon_1000.projects.nitrc.org/indi/hbn_ssi/download.html, Raw Data Accessed on Dec 15, 2016.

3.1.3 Segmentation

Once Coregistration is complete, the next pre-processing step would be Segmentation. This is a process where SPM sorts out different tissue types. The model used by SPM for segmentation implements five tissue probability maps which are already registered to the standard MNI template and then classify tissue types by registering them to these already

defined maps. What that means is that the grey matter from the data is registered to the grey matter probability map and so on for white matter, CSF etc. Figure 3.2 is an output from the segmentation stage visualized using SPM12.

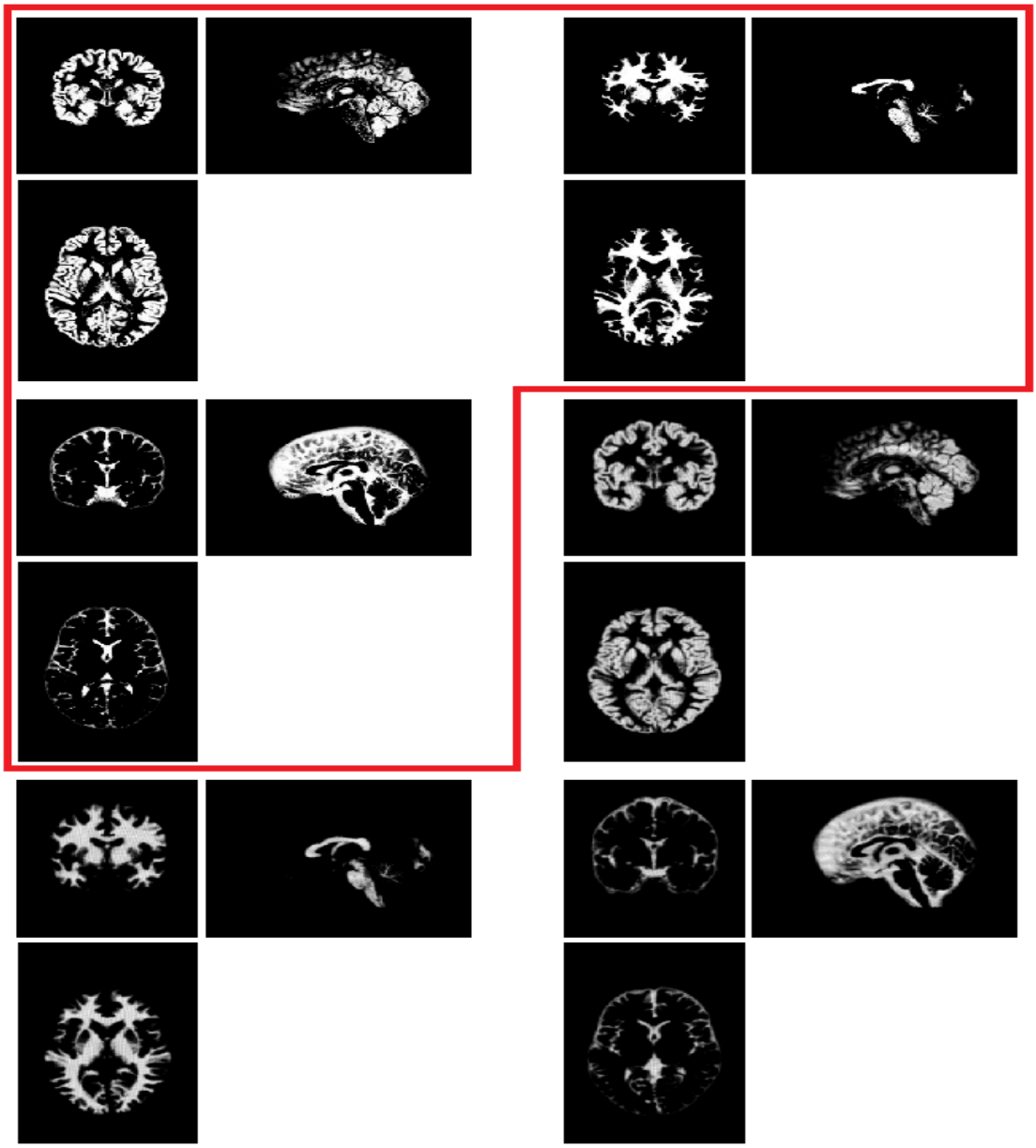

Figure 3.2 The tissue classes from native and spatially normalized space after segmentation for a single subject from a single session. The red boundary was drawn around the native tissue classes.

Source: http://fcon_1000.projects.nitrc.org/indi/hbn_ssi/download.html, Raw Data Accessed on Dec 15, 2016

3.1.4 Deformations

The segmentation step produces a deformation field as an output with a prefix ‘y_x’. This is an advanced step in SPM which allows the user to utilize the deformation field while the functional images are being transferred to the standard MNI template. There are several options that must be selected and their values properly assigned for this step to work. The input for the Composition field would be the Deformation Field, which for the current study, is named ‘y_T1.nii’ and the Voxel size and Bounding Box must also be initiated. The voxel size must be a ‘1 x 3’ matrix while the bounding box is a ‘2 x 3’ matrix. The voxel size for the current study was assigned as 3 mm x 3 mm x 3 mm. The bounding box had the same parameters as that of the standard MNI template.

After a few more adjustments the process is run and eventually the normalized image would be named ‘wx.nii’. For the current case it is ‘wrREST.nii’. The end of this step would be followed by linear regression of PCA (Principal Component Analysis) components from WM and CSF and six motion parameters from this new ‘w_x.nii’ file.

3.1.5 CSF and WM Regression

The BOLD activity in fMRI is expected to originate from the grey matter because that is where majority of the neuronal cell bodies are. The cell bodies consist of mitochondria and ATP (Adenosine Tri Phosphate) and other cellular organelles. However mitochondria and ATP are responsible for breaking down glucose by consuming oxygen. So the metabolic activity that BOLD responses depends on, occur in cell bodies which are present in grey matter. White Matter consists majorly of myelinated fatty lipid layers. CSF is a fluid that sustains the mechanical balance of the brain and provides an immunological barrier. So it is not expected that there would be any major brain activity

in the WM and CSF areas. Therefore, a cleaning of these signals is required so they do not interfere with the actual signals of interest from the grey matter.

In order to reduce these nuisance signals, first probability maps of CSF and WM generated and thresholded at $\rho > 0.99$. A Principal Component Analysis was run on the time series of these probability maps. The first five PCA components were selected from each of the CSF and WM, respectively and they were selected as regressors in a linear regression model. As per cleaning is concerned, the motion parameters from the Realignment step also need to be regressed out. So a total of sixteen regressors were used in the regression model - six Motion Parameters, five PCA Components from WM and five PCA Components from CSF. It was applied on the output dataset of the Deformation step. This process is repeated for REST, INSCAPE and MOVIE condition. One of the outputs of the linear regression is the residual matrix. This matrix was then regenerated into a 4D matrix and converted back to a '.nii' 4D image. Once this was done for all the subjects of all sessions, the images were ready to undergo any statistical analysis. But before that it is worth mentioning that the first and last five time points were cut-off from each dataset so all the conditions for each subject in all the sessions had a consistent 390 time points. It is worth mentioning that later in the book the linear regression step mentioned in this section will be addressed as the first level regression. It is mainly done to avoid confusion because there will be a secondary regression discussed later in this chapter.

3.2 Time Series Extraction

Time series extraction is required to perform further analysis after the pre-processing steps. It can be voxel wise or average ROI wise time series depending on the method chosen for extraction. A voxel wise time series was extracted for the task conditions. These time series were then used for the secondary regression of consistent task effect of all other subjects from a single subject across session and between subjects. The details on how this was done for each subject will be discussed in Section 3.3.

For estimating the functional connectivity and consequently performing a paired *t*-test between TASK vs REST conditions, average ROI wise time series were extracted. However, a number of steps need to be completed before ROI wise time series can be extracted. But the primary step is to create the ROIs and modify the masks for functional image compatibility. It will be discussed in the next section. Although the voxel wise time series was mentioned earlier, the ROI creation part will be discussed first. The two sub-sections of time series extraction will follow after that in the right order.

3.2.1 Network-Wise ROI Creation

It was mentioned earlier that Power's 264 ROIs were used for the current study. The MNI coordinates for each of the ROIs were arranged according to the brain networks. These ROIs were created using AFNI (Cox, 1996). Once the ROIs were created they were separated into 264 individual masks. However, these new ROI masks were created from a high resolution anatomical base. The resolution of these masks had to be reduced to match the resolution of the functional images. It was done because the time series will eventually be extracted from the functional images using these same ROIs. Both the ROI masks and the functional time series images should have the same resolution. Once the

ROI masks are ready, ROI wise time series extraction is easily accomplished. Figure 3.3 shows the changes in resolution of the ROI masks as it was brought down to match the functional resolution. The first row has the masks in high anatomical resolution and the second row in low functional resolution. Note that only ROIs present in a certain slice from each orthogonal plane are shown. They would not count up to 264 in Figure 3.3. The color in the masks corresponds to an arbitrary number assigned to each network it represents.

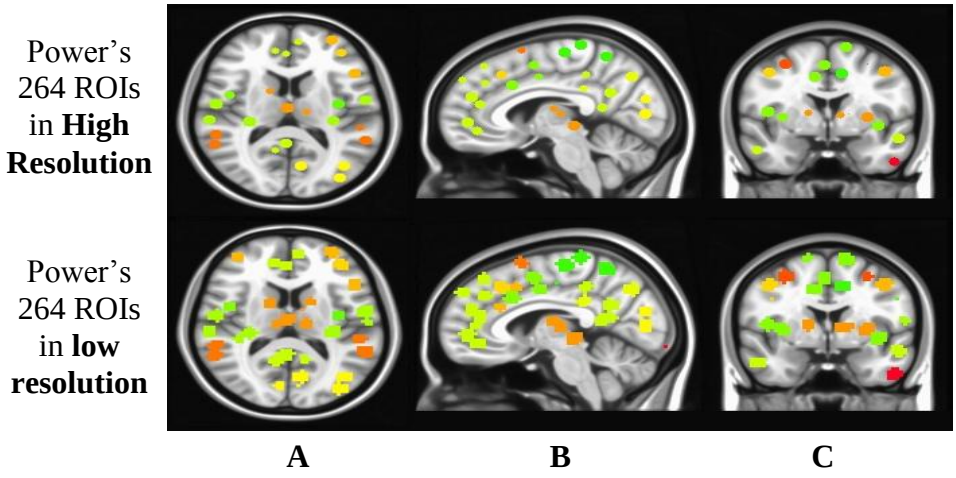

Figure 3.3 Power's 264 ROIs created initially with high anatomical resolution (first row) and then reduced to match the functional image resolution (second row). Masks with both resolutions are presented in **A**. Axial View; **B.** Sagittal View; **C.** Coronal View.

Source: http://fcon_1000.projects.nitrc.org/indi/hbn_ssi/download.html, Raw Data Accessed on Dec 15, 2016

3.2.2 Voxel Wise Time-Series Extraction

There are two methods of secondary regression applied on the task conditions in this study. The method involves a linear regression model. The consistent effect of task present in all the subjects at the group level was regressed from the subject undergoing regression, both across session and between subjects. The aim was to bring the tasks as

close to resting state conditions as possible so they can be compared using a paired *t*-test. To achieve that, the time series of the consistent task effect was regressed from each voxel of the subject undergoing the regression. This part of the analysis was done in MATLAB. Since there were 12 subjects per session and 12 sessions per subject, the number of regressors was eleven for each subject undergoing secondary regression (n = 12 - 1). This means voxel wise time series extracted from all other eleven subjects were regressed out of each voxel of the twelfth subject. The residual matrices from this linear regression would then be regenerated into 4D '.nii' image files and then the ROI wise time series were extracted from these newly regressed images.

3.2.3 ROI Wise Time-Series Extraction

This is a relatively easy and faster method once the ROI creation step is complete. The average time series from each ROI was extracted using AFNI and the values were stored in single '.1D' files. So each of the three conditions had 264 '.1D' files each from a separate ROI. These files were later loaded in MATLAB as a batch and combined for each of the functional images. This generated a matrix of 390 x 264 for each subject per condition per session where the rows represent the number of time points and the columns are specific ROIs from where the time series was extracted from. It was mentioned in the previous section that after the secondary regression the regenerated images underwent the ROI wise time series extraction. However, time series was extracted from REST after only first level regression and INSCAPE and MOVIE after secondary regression.

3.3 Secondary Regression

The two secondary regression methods applied in the current study has already been introduced in the first chapter and the previous sections of this chapter. The aim was to verify if the task effects were regressed out, would they approach resting state conditions. Each subject underwent two task conditions and one REST condition. Each subject, therefore, had three sets of functional images each with 400 time points (390 after time point cutoff). ROI wise time series were extracted for two sets of functional images (INSCAPES and MOVIE) after they have passed both the regression stages. The next two sub sections will elaborate on how the secondary regression was performed on the task conditions.

3.3.1 Regression of Subjects Across Sessions

This regression step was applied on a single subject across multiple sessions. Each subject had 12 sessions of data. If regression was being applied on INSCAPE dataset of Subject01 from Session1, then the regression model would have 11 regressors with voxel wise time series of all the other 11 sessions of Subject01 INSCAPE data. Similarly, if it was done on Subject03 from Session1, the regressors would have all other Subject03 session voxel wise time series excluding Session1. This process was repeated for all 12 subjects. The same method was also applied on the MOVIE task. The motivation for this method came from the aim to look for individual variability in functional connectivity of an individual subject undergoing multiple sessions.

The regression model follows the basic linear regression equation:

$$\boldsymbol{r = YX} \tag{3.1}$$

where $\boldsymbol{r}$ = the residuals after regression, $\boldsymbol{Y}$ = the observed responses and for the current study it would be the voxel wise time series of a particular subject from a particular session and $\boldsymbol{X}$ = the independent predictors which for the current study would be the regressor matrix consisting of all other sessions' voxel wise time series for the same subject in $\boldsymbol{Y}$. For the current study, $\boldsymbol{Y}$ would consist of 'n x 1' vectors where n = 400, the number of time points consisting of time series values from a single voxel. $\boldsymbol{X}$ would consist of 'n x p' vectors where n is the same as n in $\boldsymbol{Y}$ and p is the number of regressors, i.e. p = 11.

Figure 3.4 is a schematic diagram of this regression method. The top part is used to show how INSCAPE dataset of other sessions (Top Right) are regressed from the INSCAPE dataset of Subject01 from Session1 (Top Left). The bottom part represents an expanded view of what is going on during the regression at the matrix level. The regressor matrix consists of voxel wise time series of all other sessions (Bottom Right). The blue line with connecting dots is used to represent the relationship between the regressor matrix and responses in voxel wise time series of INSCAPE from Session1 (Bottom Left).

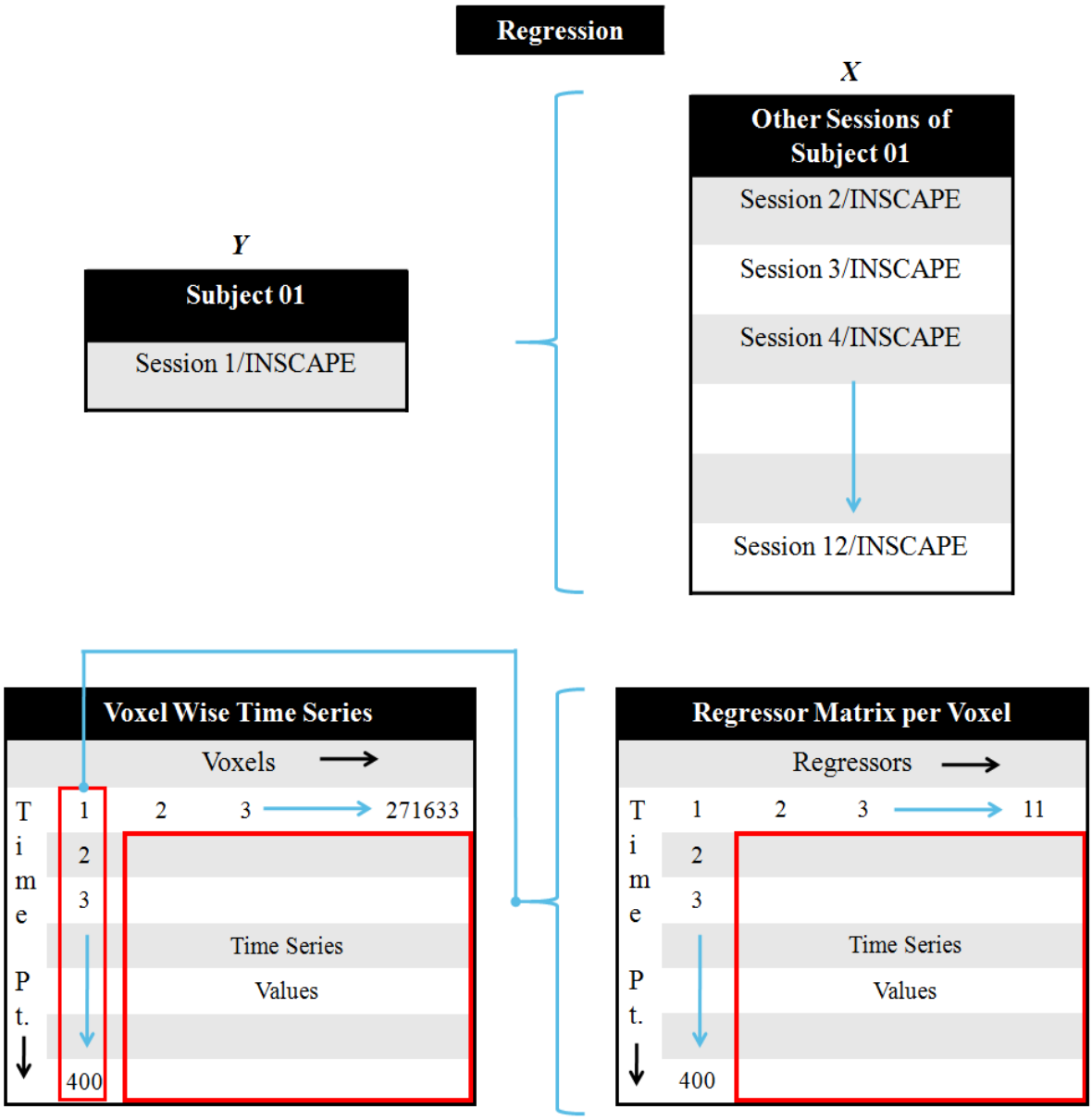

Figure 3.4 A schematic diagram for the method applied for regression of a single subject. across sessions. The vertical axes labels represent time points as columns and the horizontal axes labels represent voxels and regressors respectively for both blocks at the bottom of the figure.

The red rectangular bounding box on both of the blocks at the bottom part of the figure represents the actual dataset with all the time series values. The horizontal and vertical axes labels were added to show how the matrices are actually arranged. For each

voxel time series of Subject01 from Session1 (longitudinal red bounding box), an entire matrix of size 400 x 12 is passed as the regressor. The reason it is 400 x 12 is because there are 11 regressors and an additional column of 'ones', which is required as an input to account for the constant term. This is mainly because the *regress* command used in MATLAB uses the simplistic equation discussed in this section. It does not account for the intercept of the linear equation. This process is repeated for all 271633 voxels on the bottom left block which is the total number of voxels in the functional image of the INSCAPE condition. This method is also applied to the MOVIE dataset in the exact same manner.

3.3.2 Regression Between Subjects of a Single Session

This regression method was applied between subjects of the same session. The motivation behind this regression strategy came from looking into inter-subject variability in functional connectivity for task conditions. While the principle of regression remains the same, the regressor matrix now consists of other subjects' voxel wise time series. Since INSCAPE was used to show across session regression, MOVIE will be used for this section. There is no special reason for doing so, it is simply done to show that both models work for both the task conditions. If the voxel wise time series from Subject01 from Session1 would undergo regression, the regressor matrix would be formed in the same manner as it was done in Section 3.3.1. However, instead of having the voxel wise time series of all other sessions of the same subject, it will be the voxel wise time series of all other subjects of the same session. Consequently, $\boldsymbol{X}$ would consist of regressors from Subject02 to Subject12 of Session1. Since the number of subjects per session is twelve (n = 12), $\boldsymbol{X}$ would still consist of 11 regressors (n = 12 -1) with one

additional column of ones (400 x 12). Similarly, if Subject03 of Session1 would undergo regression, the regressor matrix would be formed of voxel wise time series of Subject01 and all other subjects except Subject03 of Session1. This process is repeated for all subjects of the same session and likewise for both task conditions. Figure 3.5 is a very similar daigram as Figure 4.4 and most of the blocks of the diagram are self explanatory if referred back to the description of Figure 3.4 in Section 3.3.1. Note the only difference would be the different subjects (Upper Right) which have replaced the different sessions in Figure 3.4.

3.4 Group Level Paired *t* – Test

Once all the regression steps were done and the time series have been extracted, statistical analyses and hypothesis tests were performed on the dataset. The functional connectivity matrices were generated and they were Fisher's Z transformed. These new Z – transformed matrices were used to perform a paired *t* – test between REST and TASK conditions. The paired *t* – test was performed in MATLAB. The aim to perform this test was to look for ROIs which show statistically significant differences between REST and INSCAPE and REST and MOVIE after both of these task conditions have passed the two secondary regression steps. This means there would be four paired *t* – tests altogether. Table 4.1 summarizes the paired *t* – test categories.

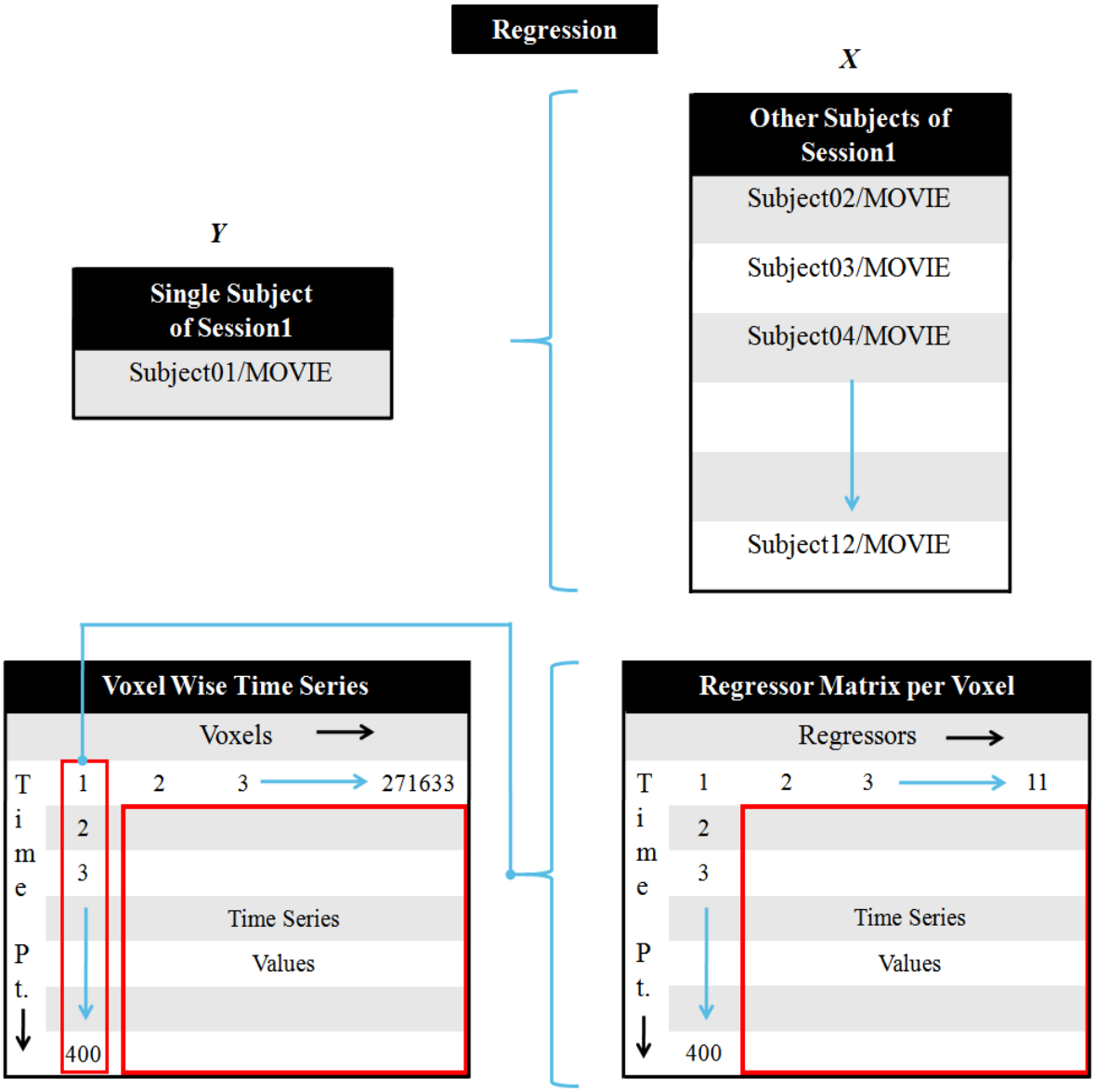

Figure 3.5 A schematic diagram for the method applied for regression of a single subject between subjects of the same session. The vertical axes labels represent time points as columns and the horizontal axes labels represent voxels and regressors respectively for both blocks at the bottom of the figure.

Table 3.1 Summary of Paired *t* – tests Performed Between TASKs and REST

Paired *t* – test Between Conditions after Regression Across Session	**CONDITION 1**	**CONDITION 2**
	INSCAPE	REST
	MOVIE	REST
Paired *t* – test Between Conditions after Regression Between Subjects	**CONDITION 1**	**CONDITION 2**
	INSCAPE	REST
	MOVIE	REST

The paired *t* – test command in MATLAB follows a simple equation:

$$[\boldsymbol{h}, \boldsymbol{p}] = \boldsymbol{ttest}\ (\boldsymbol{x}, \boldsymbol{y}) \tag{3.2}$$

where, $\boldsymbol{h}$ = the result of the hypothesis, $\boldsymbol{p}$ = the $\boldsymbol{p}$ – values associated with the results of hypothesis and $\boldsymbol{x}$ and $\boldsymbol{y}$ are vectors of the two conditions being compared, which in this case could be any of the pairs from Table 3.1. This particular command tests the null hypothesis and gives outcome in the form of $\boldsymbol{h}$ and $\boldsymbol{p}$ showing whether the null hypothesis is true or rejected for each of the 264 ROIs between the two conditions. The $\boldsymbol{h}$ values are binary in nature. A 0 means the null hypothesis is true which means there is no statistically significant difference in the ROIs of the two conditions. A 1 means the null hypothesis has been rejected and therefore there is a difference in the ROIs. The functional connectivity matrices are 264 x 264 in size.

All pairs mentioned in Table 3.1 generated four different sets of $\boldsymbol{h}$ and $\boldsymbol{p}$ value matrices. However, the concern for multiple comparisons with False Discovery Rates

(FDR) remains and so an FDR correction step was necessary. The next section will elaborate on the method applied for FDR correction before the final results were obtained.

3.5 FDR Correction

The FDR Correction is a method of controlling false discoveries in cases of multiple comparisons. For the current study, it was done using MATLAB. The paired *t* – test in MATLAB has a default $\boldsymbol{p}$ – value threshold of $\boldsymbol{p} < 0.05$. This threshold was fed into the FDR correction algorithm and the FDR corrected threshold was found from the $\boldsymbol{p}$ – value matrices of the paired *t* – test. The FDR corrected thresholds were very strong and indicated only one ROI pair per pair condition in Table 3.1. Eventually, an arbitrary threshold of $\boldsymbol{p} < 0.0005$ was chosen to look for significant differences in ROIs for all the four pair conditions. These FDR corrected results will be presented and discussed in Chapter 5. The bar graphs in Chapter 5 were created to show the directionality of the conditions i.e. whether the difference is more in REST or INSCAPE and so on for other conditions. In order to show the directionality, the values from the mean connectivity matrices for each condition and their Standard Error of Mean had to be found first. Since the ROI pairs showing significant differences at $\boldsymbol{p} < 0.0005$ were already known, these same ROI pairs were found in the mean functional connectivity matrices for each condition pair. The Standard Error of Mean was found using the following formula:

$$\boldsymbol{SEM} = \frac{\boldsymbol{\sigma}}{\sqrt{\boldsymbol{n}}} \tag{3.3}$$

where, $\boldsymbol{\sigma}$ = standard deviation of the Fisher's Z transformed correlation coefficient values from $\boldsymbol{n}$ = 12 subjects for the same ROI pairs found for $\boldsymbol{p} < 0.0005$. The mean connectivity matrix values (Fisher's Z transformed Correlation Coefficient values) of REST, INSCAPE and the SEM values were listed in a spreadsheet and finally the bar graphs were generated for each condition pair mentioned in Table 3.1.

CHAPTER 4

FUNCTIONAL CONNECTIVITY

Functional Connectivity measures may provide information on understanding whether the brain regions function locally or are they distributed and somehow coordinate with each other across different regions. It was shown that while 'functional specialization' exists in local regions for a particular mental activity, a 'functional integration' was also required to coordinate those regions for understanding how the brain performs compound mental functions (Friston, 1994).

Functional Connectivity is an estimate of how strongly neurophysiological events are temporally correlated between each other while they occur in distinct geographically distant spaces (Friston et al, 1993a). Another concept called 'effective connectivity' was also discussed in that same study. It is an estimate of how much one region directly or indirectly influences the other region or have a shared influence on the other. The current study is based on the functional connectivity changes that can be observed in task state compared with resting state. As such, functional connectivity maps were generated for all three conditions and all the analysis that followed are based on the functional characterization of ROIs associated with organized networks of the brain. The next section discusses some of the aspects, advantages and disadvantages of resting state and task state functional connectivity.

4.1 Resting State And Task Activation Functional Connectivity

For sustaining neurons functioning at resting state conditions, the brain uses up about 20% of the whole body's energy (Shulman et al., 2004). It is therefore quite obvious why paradigms relying on the metabolic activities in the brain can show spontaneous activations at resting state situations. In task state, neuronal activations however consume much less energy. The metabolism increase is < 5% and so during a task condition only a certain region of the brain that is coherent to the task can be studied (Raichle et al., 2006). It may not provide sufficient information on how the entire brain operates. Resting State data allows the use of the same dataset to study several regions of the brain. Resting state connectivity also comes with better SNR because, in task conditions, about 80% of the changes in BOLD signal is averaged out and discarded as noise (Fox et al., 2007). On the other hand, this noise becomes the signal of interest in resting state conditions. Comparatively, the task paradigm allows easy detection of different states of the same region e.g., 'on' and 'off', 'active' or 'inactive' and 'reluctant' or 'excited'. The block design experiments provide relative advantages in understanding the functional connectivity of a certain brain region over resting state conditions.

There are several methods of estimating the functional connectivity for resting state and task conditions. One of the two methods used in the current study, is a seed based correlation generating correlation coefficient maps. The other method was used to visually inspect the independent functionally connected brain regions. It is known as Independent Component Analysis (ICA). The next two sections will discuss these two methods.

4.2 Correlation Coefficient Maps

Seed Based Correlation is a commonly used method to study functional connectivity in the brain. Usually, a brain region is selected a priori and then average time series from that ROI or voxel wise time series are generated and a correlation is run for time series across the whole brain to find which other regions are temporally correlated with the seed region. However, the current study implements an ROI-based average time series correlation approach.

There are several standardized atlases with whole brain ROI-based models that are established in the field of neuroscience today. Dosenbach's 160 ROIs, Craddock's 200 ROIs are very common and usually used for many functional connectivity and parcellation analyses. Power's 264 ROIs (Power et al., 2011) based on the MNI atlas was used for this study. This part of the process was entirely done using AFNI. Average time series were extracted from the individual ROIs and correlated with voxels from the whole brain. The correlation was performed using MATLAB and both subject level and group level mean connectivity maps were generated. The correlation 'r' values were Fisher's Z transformed because it provides a normal distribution with a known standard error. The connectivity map figures are presented in Chapter 5. Generally, if there are *n* number of ROIS, the resultant connectivity map would have an *n* x *n* matrix. Since there are 264 ROIs used in the current study all the correlation maps have a matrix size of 264 x 264.

It works with simple matrix operations. As mentioned in the previous chapter, the functional data were customized to have 400 time points for each condition. The first and last five time points were cutoff to account for T1 relaxation effects and all subjects for each task condition then had a consistent 390 time points through and across all sessions.

Essentially, the time series for each subject for each condition had a matrix size of 390 x 264. This means each of the 264 ROIs had an average time series of 390 time points where the time points are the rows and the ROI numbers are the columns. Therefore, when each of the 264 columns in that matrix underwent pair-wise linear correlation the consequent matrix size ended up being 264 x 264.

Figure 4.1 below is a simple illustration of this method for a visual understanding. Only a few steps of pair-wise correlation are presented here with a 5 x 4 matrix consisting of arbitrary alphabetic elements. It shows how column 1 is correlated with column 2 and then column 3 and 4 respectively. The same process is repeated for all the other columns. Thus the result of a pair-wise correlation of a 5 x 4 matrix is a 4 x 4 matrix. The correlation coefficients are represented with double subscript notation to hint the column pairs from which they were derived. Note the red rectangular box along the diagonal of the correlation coefficient matrix. It represents correlation values of a column correlated with itself. Hence, all the elements along this diagonal will have a value of '1'. Consequently, these diagonal values are removed when doing further analysis like FDR (False Discovery Rate) correction since an ROI will always correlate with itself with a maximum value of 1.

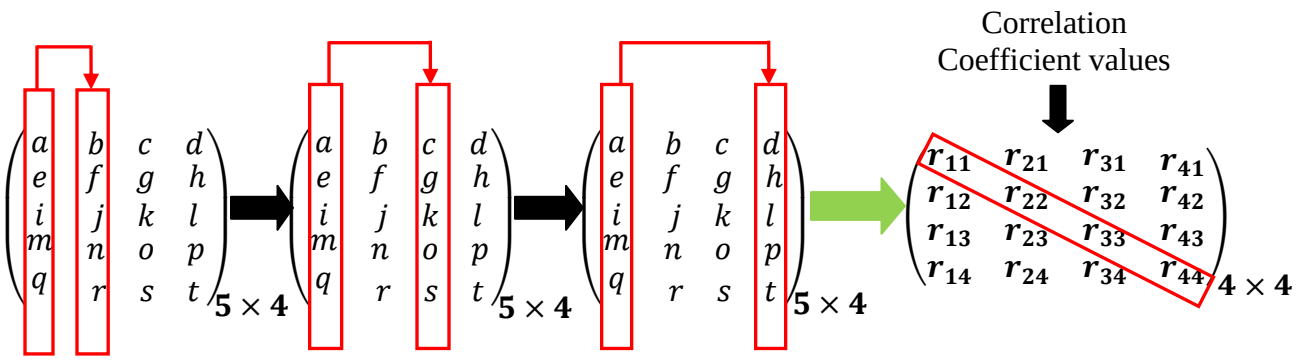

Figure 4.1 A simple representation of the correlation method used for deriving the subject level functional connectivity of the different task conditions and rest. The longitudinal rectangular red boxes represent the column pairs undergoing Pearson's correlation. The diagonal red box has correlation coefficient values of 1.

In order to convert these 'r' values to Fisher's Z values, a simple formula can be utilized:

$$Z = \frac{1}{2}\ln\frac{(1+r)}{(1-r)} \tag{4.1}$$

where **Z** = Fisher's Z transformed values, **r** = Pearson's correlation coefficients. For all further analysis involving the functional connectivity of the three conditions, the Fisher's Z values were used instead of the r values. The group level mean functional connectivity was also estimated by averaging the functional connectivity matrices for all 12 subjects from session one and across all twelve sessions.

4.3 Independent Component Analysis (ICA)

This is a popular data driven method used in the field of neuroscience to estimate functional connectivity. In the initial fMRI stages, Principal Component Analysis was

used because it is easy to implement. But the issue with other alternative methods is they assume the data follows Gaussian distribution. Practically, data do not often follow the Gaussian distribution. This leads to the choice of ICA. ICA has two important features that make it very suitable for this kind of analysis – it derives components that are not only 'statistically independent' but also 'non-gaussian' in nature (Hyvarinen et al., 2001). ICA is proximately relevant to a method called Blind Source Separation (BSS). The motivation behind the method comes from a famous principle known as the 'Cocktail Party Problem'. The concept of how ICA is based on the BSS and the 'Cocktail-Party Problem' will be discussed next.

The 'Cocktail-Party Problem' assumes that there are three guests speaking simultaneously like in any cocktail-party but there are three individual microphones to record their speech. Obviously if the recorded signals are played in a speaker it will be a mixed signal of three unique source signals. It should be clear that assumption of three guests and microphones is just to set an example. In fact, it could be any number of speakers with equal number of sensors to detect their speech. Of course, the weight by which each signal is received by a microphone varies depending on how far that microphone is from the sources and what is the direction at which they are delivering the speech, in other words, from which direction the speech is arriving to the microphone. There could be many other factors but for simplicity they are assumed to be negligible. The idea is to separate the original signals from the mixed signals received from each microphone.

Figure 4.2 is a simplified illustration of the 'Cocktail-Party Problem'. The waves shown in the diagram are a simple schematic to represent the mixed signals. They are not

actual speech signals. The speech block in the middle of the three guests is used to symbolize their conversation and it is a mixture of three independent signal sources each coming from a unique guest. The shape and amplitude of each wave are shown to be different to note that they are all weighted differently due to the distance of travel and angle of reception for the speech at the microphones.

The three recorded mixed signals or what can be called as the observed signals can be represented by three instantaneous variables, $\boldsymbol{m_1(t)}$, $\boldsymbol{m_2(t)}$ and $\boldsymbol{m_3(t)}$ with $\boldsymbol{t}$ representing the instantaneous time. Each of these individual mixed signals is a weighted sum of the audio signals of each unique guest, $\boldsymbol{g_1(t)}$, $\boldsymbol{g_2(t)}$ and $\boldsymbol{g_3(t)}$. But all the mixed signals are weighted differently due to distances between source and receiver and other factors, a coefficient must be taken into account to represent these factors. They can be represented by the three following equations (Hyvarinen Aapo et al., 2001):

$$\boldsymbol{m_1(t) = d_{11}g_1(t) + d_{12}g_2(t) + d_{13}g_3(t)} \quad (4.2)$$

$$\boldsymbol{m_2(t) = d_{21}g_1(t) + d_{22}g_2(t) + d_{23}g_3(t)} \quad (4.3)$$

$$\boldsymbol{m_3(t) = d_{31}g_1(t) + d_{32}g_2(t) + d_{33}g_3(t)} \quad (4.4)$$

where $\boldsymbol{d_{11}\ldots d_{33}}$ represent the aforementioned weighting factors. Considering BSS and ICA the original signal, i.e. the speech from one of the guests in the cocktail-party problem would be the 'source' in BSS and 'Independent Component' in ICA. The 'Blind' in BSS is meant to emphasize that the knowledge about the mixing signal is so less, that the person applying the method has to make very weak assumptions to derive the original signals. These equations lead on to the concept of independent component analysis.

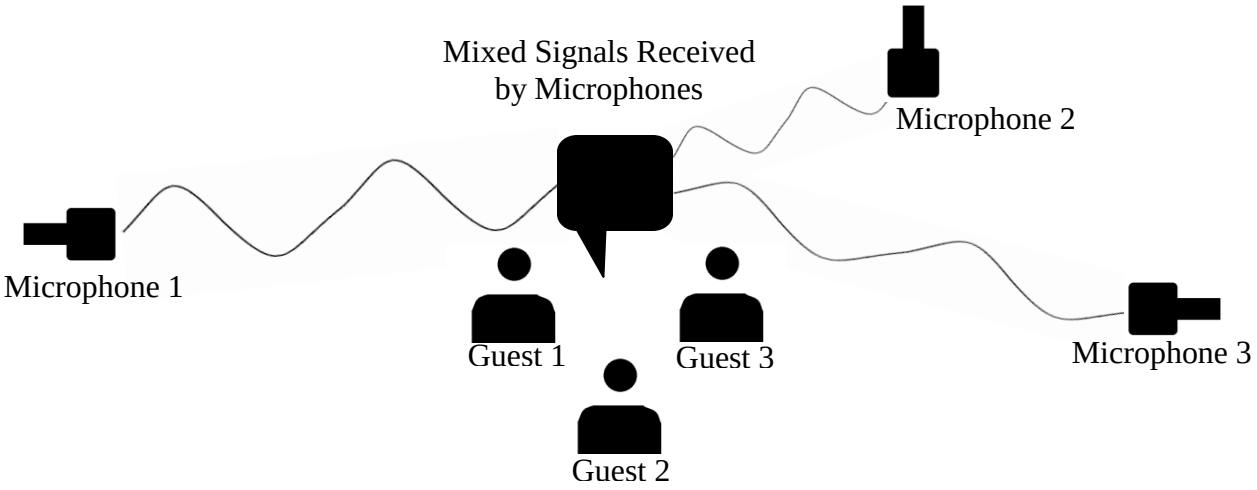

Figure 4.2 A simplified illustration of the Cocktail-Party Problem with three guests having a conversation and three microphones receiving mixed signals.

If $x_1 \ldots x_n$ are n observed random variables which are linearly related to n random variables $s_1 \ldots s_n$, they can be represented with a very similar looking equation:

$$x_i = a_{i1}s_{i1} + a_{i2}s_{i2} + a_{i3}s_{i3} + \cdots + a_{in}s_{in} \tag{4.5}$$

where $i = 1, 2, 3, \ldots n$ and all real coefficients $a_{i1} \ldots a_{in}$. This is the generalized ICA equation and so it does not entail the instantaneous time, t. This is because the mixed signals from the cocktail-party problem could be just one such random variable in the independent component analysis. There could be other non-instantaneous random variables too. Usually for convenience and easier understanding of ICA, instead of implementing the clumsy sum equations a vector matrix is used. So all the $x_i \ldots x_n$ could be taken as a set of elements in a matrix, x. Similarly, for all the $s_i \ldots s_n$ as s and likewise A, the mixing matrix, for all a elements. Now it can be represented as a single equation:

$$\boldsymbol{x} = \boldsymbol{As} \tag{4.6}$$

As was mentioned before, ICA works for data that have non-gaussian distribution. In fact ICA depends on two assumptions to work. The independent components, which in the current study would be the independent BOLD responses from neurons, are statistically independent and their distribution is non-gaussian which is usually the case with these datasets. That is why ICA is very effective for deriving the functional connectivity in fMRI studies. Another important point to discuss would be the exclusion of error term $\boldsymbol{e}$ in standard ICA. Hence, it does not give the error term. However, FSL MELODIC (http://fmrib.ox.ac.uk/analysis/research/melodic/) was used in the current study to derive the spatial and temporal maps and it uses a modified probabilistic model that includes an error term to isolate the noise (Beckmann et al., 2004). The probabilistic ICA model equation is:

$$\boldsymbol{x} = \boldsymbol{As} + \boldsymbol{e} \tag{4.7}$$

where, $\boldsymbol{e} \sim \boldsymbol{N}(0,\boldsymbol{\sigma})$. It means the error term $\boldsymbol{e}$ is normally distributed.

FSL MELODIC (http://fmrib.ox.ac.uk/analysis/research/melodic/) can perform Concatenated ICA (cICA) or Tensor ICA (tICA) respectively. In the current study both cICA and tICA were performed for task conditions, INSCAPES and MOVIE before any secondary regression was performed to the dataset. However, doing a tICA is not plausible for Resting State condition so only cICA was performed for REST.

For all spatial components, the data needs to be organized into a two dimensional dataset. For concatenated ICA, all the data are arranged into a gigantic two dimensional stack where each dataset is concatenated on top of the other. Then a single 2D ICA is run on this stack to look for spatial patterns.

For tensor ICA, the entire data set is arranged into a single 3D matrix of 'time x space x subjects/sessions' block (Beckmann et al., 2005). MELODIC performs a tensor ICA to find components of task conditions that are consistent across sessions or between subjects.

For the current study, 50 components were fixed. It was constant for both concatenated (cICA) and tensor (tICA) applied to the dataset of all three conditions. The tICA was done to check if the components of INSCAPE and MOVIE show consistency across sessions and between subjects and also to analyse those time series for future research which could not be completed in the current study. Initially cICA of REST, INSCAPE and MOVIE generated a set of maps and then, tICA of INSCAPE and MOVIE generated a set of maps. An overlapped common map comparison was done with each task conditions' cICA and tICA to see how defined their maps are and whether they exhibit total voxel overlap or not. This means each cICA map of INSCAPE that is common to its tICA INSCAPE map was compared. Similarly each cICA map of MOVIE was compared to its tICA map. It is important to note that not all maps were generated for the tICA maps especially for the MOVIE condition within the 50 components limit and hence the common map comparison. Table 4.1 below summarizes the individual ICA Maps and their corresponding comparisons that were mentioned above. The images to the generated maps can be found in Chapter 5.

Table 4.1 Summary of ICA Map Generation and Comparison per Condition

Individual Maps for all Three Conditions	**cICA**	**tICA**
	REST	–
	INSCAPE	INSCAPE
	MOVIE	MOVIE
Common Map Overlap Comparison TASK	**cICA**	**tICA**
	INSCAPE	INSCAPE
	MOVIE	MOVIE

CHAPTER 5

RESULTS

This chapter describes in detail, all the results from the current study. Subject level connectivity maps are presented and then group level mean connectivity with ICA maps and paired *t* – test results are shown at the end of the chapter.

5.1 ICA Maps

ICA maps were generated using methods discussed in Chapter 4. The two methods discussed were Concatenated and Tensor ICA. The following sections will present estimated maps for each condition. ICA maps generated from each of the conditions before any secondary regression are presented.

5.1.1 Concatenated ICA Maps of Rest

Figure 5.7 shows the independent component maps estimated from the REST dataset. The Medial Visual (MV), Sensory Motor (SM), Dorsal Attention (DA), Right Fronto Parietal (RFP), Left Fronto Parietal (LFP) and the Default Mode Network (DMN) were found. Within the 50 components limit, almost all of the major networks derived from the functional connectivity analysis for REST in Section 5.2 were confirmed in the ICA analysis. Only auditory and the salient networks seem to be absent however the auditory networks do show up for INSCAPE and MOVIE conditions. The MV network corresponds to perception and motion during vision. The SM network consists of supplementary motor area, sensorimotor cortex, and secondary somatosensory cortex (Smith et al., 2009). This network is strongly associated with action and execution

paradigm. The DA network consists of intraparietal sulcus (IPS) and frontal eye fields (FEFs) on either hemisphere. This network corresponds to attention in space, like predicting spatial cues (Posner, 1980). The RFP and LFP are the frontoparietal networks. They are strongly lateralized and mirrored in two hemispheres. The RFP corresponds to perception and pain while the LFP relates to cognition and language paradigms. The DMN network comprises the medial parietal, bilateral inferior–lateral–parietal and the ventromedial frontal cortex. It is usually deactivated in task based experiments and poses a negative contrast unlike the positive activations of other networks (Smith et al., 2009).

5.1.2 Concatenated and Tensor ICA Maps of Inscapes

Figure 5.8 shows the independent component maps estimated from the INSCAPES dataset. The group of figures on the left hand side represents the ICA maps derived from the concatenated ICA approach applied in FSL MELODIC (http://fmrib.ox.ac.uk/analysis/research/melodic/) for the INSCAPES dataset. Figures on the right side represents the tensor ICA maps of the same dataset. Section 4.3 from Chapter 4, discusses the details of how and why these approaches were applied. The tensor ICA detects the independent networks that are being activated due to a consistent task effect. Since the regression in the initial stage did not show much visible differences an approach to regress the consistent task effect time-series was strategized. The Medial Visual (MV), Sensory Motor (SM), Occipital Pole (OP), Right Fronto Parietal (RFP), Dorsal Attention (DA), Default Mode Network (DMN), Audio (AUD) and the Left Fronto Parietal (LFP) were identified from the 50 components derived from the cICA approach applied in FSL MELODIC. Similarly all the networks except for the LFP were

also estimated in the tICA approach. Compared to the MOVIE condition INSCAPES show better consistency in network activation.

The visual network OP was not observed in the rest dataset but is present in INSCAPE. It partly consists of the primary visual cortex and is formed by the conjoining of superior and inferior occipital gyri. It corresponds to cognition, language and orthography paradigms (Smith et al., 2009). The INSCAPE movie consists of music and notes. It was expected that the AUD network would show up as one of the ICA components. The auditory network consists of the superior temporal gyrus, Heschle's gyrus and posterior insular. It comprises the primary and the association auditory cortex. It corresponds to action, execution speech, cognition, perception and auditory paradigms (Smith et al., 2009).

5.1.3 Concatenated and Tensor ICA Maps Of Movie

Figure 5.9 shows the estimated cICA and tICA maps from the MOVIE dataset. The group of figures on the left hand side represents the ICA maps derived from the concatenated ICA approach applied in FSL MELODIC for the MOVIE dataset and the right side represents the tensor ICA maps of the same dataset. The Medial Visual (MV), Sensory Motor (SM), Occipital Pole (OP), Audio (AUD), Right Fronto Parietal (RFP), Left Fronto Parietal (LFP), Default Mode Network (DMN) and the Dorsal Attention (DA) networks were identified from the 50 components derived from the cICA approach applied in FSL MELODIC. However, tICA components revealed only the MV, SM, OP and AUD networks. Compared to the number of tICA maps for INSCAPES this shows that the consistent effect of task is found in fewer networks for the MOVIE condition.

Concatenated REST
ICA MAPS:

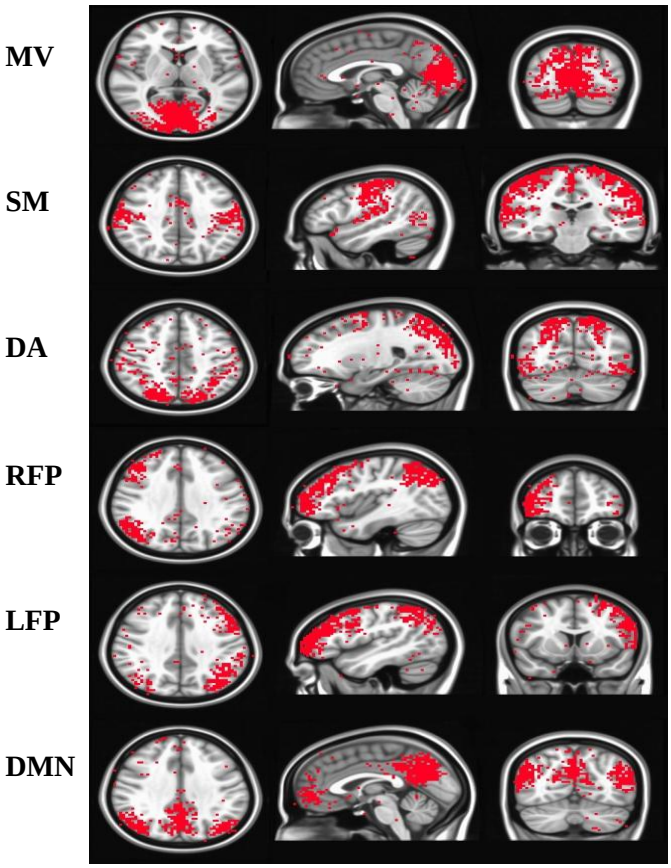

Figure 5.1 Concatenated ICA (cICA) Maps of Resting State Condition for all subjects in Session 1. The Medial Visual (MV), Sensory Motor (SM), Dorsal Attention (DA), Right Fronto Parietal (RFP), Left Fronto Parietal (LFP) and the Default Mode Network (DMN) are shown in descending order from the top.

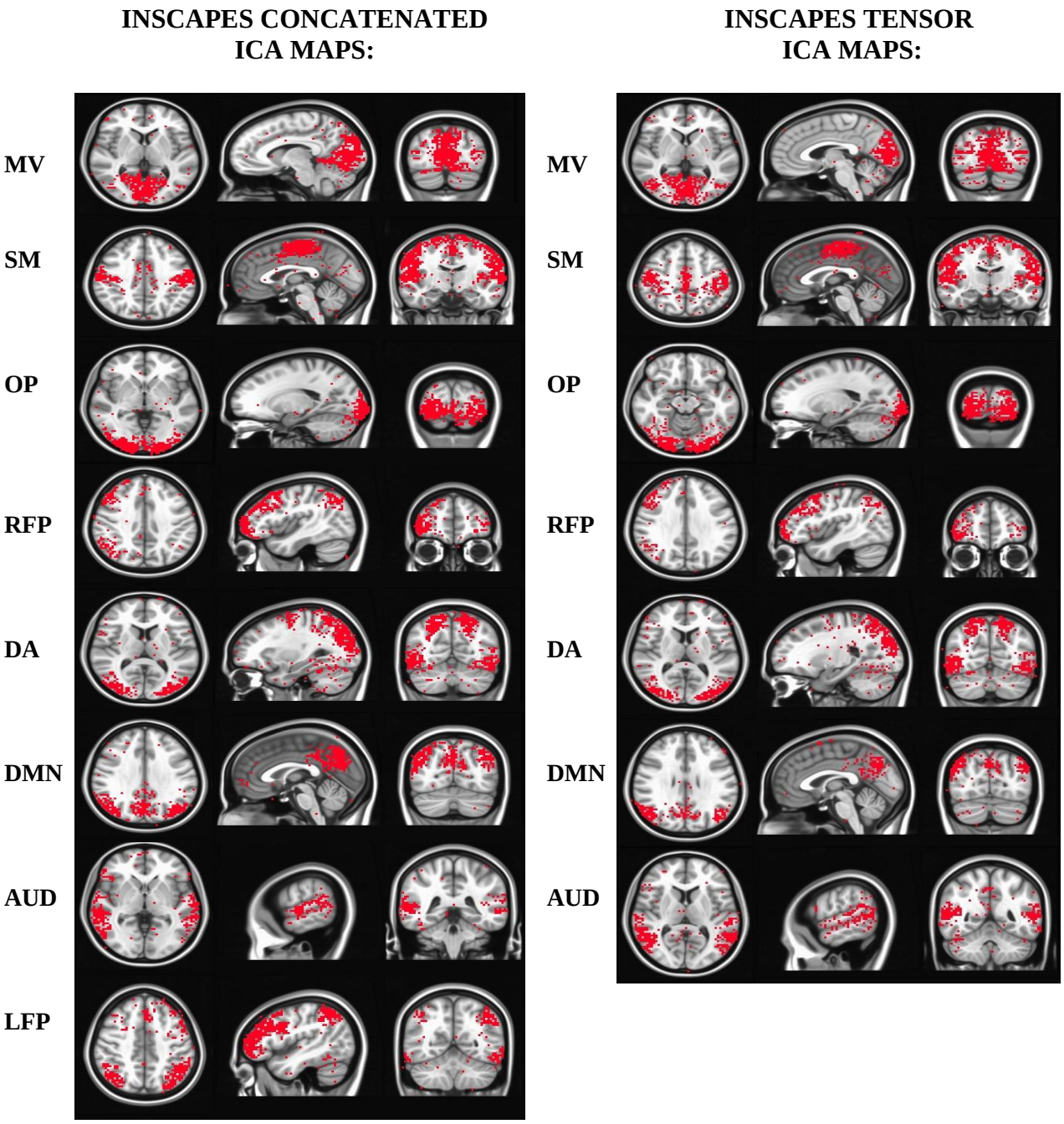

Figure 5.2 Concatenated ICA (cICA) Maps (LEFT) and Tensor ICA (tICA) Maps (RIGHT) of INSCAPES for all subjects in Session 1. The Medial Visual (MV), Sensory Motor (SM), Occipital Pole (OP), Right Fronto Parietal (RFP), Dorsal Attention (DA), Default Mode Network (DMN), Auditory (AUD) and the Left Fronto Parietal (LFP) were derived for cICA. All networks with exception of LFP were also derived for tensor ICA.

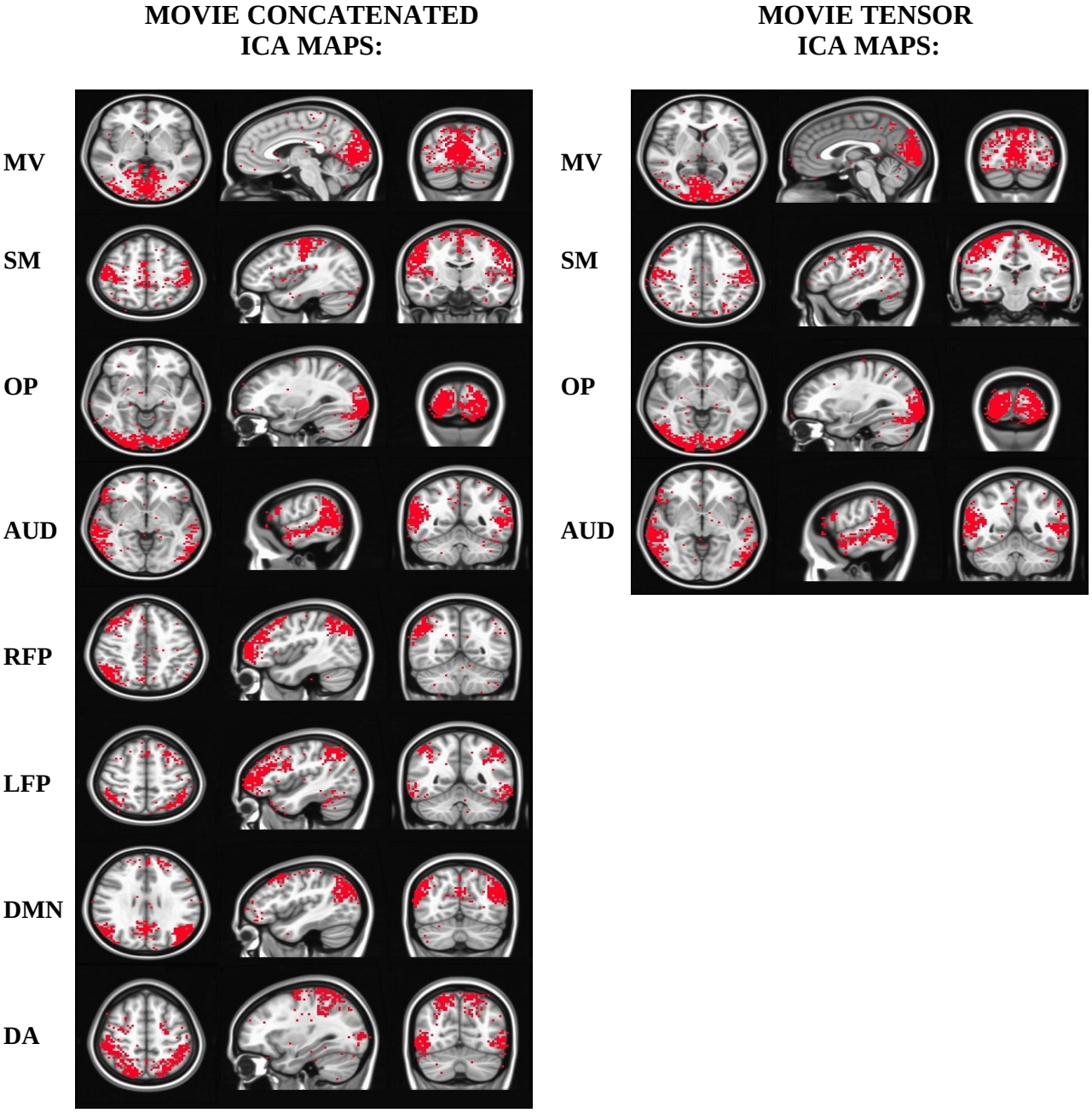

Figure 5.3 Concatenated ICA (cICA) Maps (LEFT) and Tensor ICA (tICA) Maps (RIGHT) of MOVIE for all subjects in Session 1. The Medial Visual (MV), Sensory Motor (SM), Occipital Pole (OP), Audio (AUD), Right Fronto Parietal (RFP), Left Fronto Parietal (LFP), Default Mode Network (DMN) and the Dorsal Attention (DA) networks are arranged in descending order from the top on the left hand side. The tICA generated only MV, SM, OP and AUD networks.

5.2 Subject Level Connectivity Maps

The next few sections will present the connectivity maps of all 12 subjects from Session1. They are all 264 x 264 matrices. The ROIs were arranged according to the networks defined from Power et al. 2011. As a measure of locating the networks all connectivity maps have two identical color bars, one horizontally on top and one vertically on the left of each subject's map. The color code legend is given at the bottom of the figure with each network's name on it. Note there is also another color bar on the right of each subject's connectivity map. It represents the color corresponding to the correlation value to represent the strength of correlation of ROIs within intra and inter networks respectively. The range of Fisher's Z Transformed Correlation Coefficient values represented by the color bar is -0.4 to 0.4. The same scheme is applied to represent all the different criteria of subject level functional connectivity.

5.2.1 Resting State Connectivity

Figure 5.1 shows the subject level functional connectivity of all the 12 subjects from the first session. The Resting State Connectivity was derived after the first regression step only. Each row in the figure represents three subjects. The subject number increases from left to right. For example, in the first row, it starts with Subject01 from the left and increments to Subject03 to the right and so on up to Subject12 at the end of 4^{th} row.

The networks are arranged in the following order: Somatomotor Hand (SMH), Somatomotor Mouth (SMM), Cingulo Opercular Network (CON), Auditory (AUD), Default Mode Network (DMN), Memory Retrieval (MR), Visual (V), Fronto Parietal

Network (FPN), Salient (SAL), Subcortical (SBC), Ventral Attention (VA), Dorsal Attention (DA), Cerebellar (CEB) and there were some ROIs that fall in an undefined network. The SMH and SMM basically form the Sensory Motor (SM) Network. It contributes to activations from bimanual tasks and corresponds to action-execution and perception paradigms (Smith et al., 2009). CON consists of anterior insula, dorsal anterior cingulate cortex and the thalamus. This network has shown activation for tonic alertness (Sadaghiani et al., 2015). The AUD network consists of superior temporal gyrus, precentral and postcentral gyri, inferior parietal lobule and insular regions. They cover the primary and secondary auditory cortices. This network has a range of functions like language, speech, action, execution, cognition, perception and audition.

The DMN is a big network with the highest number of ROIs comprising it. It consist of a number of brain region including posterior cingulate cortex, precuneus, medial prefrontal cortex, angular gyrus, and dorsal medial pre-frontal cortex. It is usually inactive during task and inherently active during wakeful rest. It has been shown that DMN is active when a person thinks about himself, about others and the future (Buckner et al., 2008). The MR network is composed of the cingulate gyri and the precuneus. This network shows activation individually and in conjunction with DMN during memory retrieval and episodic memory (Sestieri et al., 2011). The Visual network primarily consists of ROIs from the occipital lobe. It covers the three visual networks - Medial Visual, Occipital Pole and Lateral Visual areas. Their functions vary from perception of visual motion to cognition of space and orthography (Smith et al., 2009). Subjects 03, 08 and 09 show the strongest correlation in the visual network from the entire group in Figure 5.1. The FPN are mirrored to each hemisphere of the brain. It consists of Right

Fronto Parietal (RFP) and Left Fronto Parietal (LFP) networks. One corresponds to perception and pain while the other to cognition and language, respectively (Smith et al., 2009). The SAL network consists of anterior insula and dorsal anterior cingulate cortex. It also consists of subcortical structures - amygdala, ventral striatum and the substantia nigra. Functions associated with SAL network includes communication, social behavior, self awareness, emotion and cognition (Craig, 2009, Mennon et al., 2010). The SBC network consists of thalami, extra-nuclear regions and lentiform nuclei. The basal ganglia have been shown to contribute in higher cerebral processes that regulate cognition, decision making and planning complex strategies (Houk et al., 2001, Seger et al., 2006). The DA and VA networks conjointly contribute for attention. The DA consists of Intra Parietal Sulcus (IPS) and the Frontal Eye Field (FEF). The VA network consists of the temporoparietal junction (TPJ) and the ventral frontal cortex (VFC). It shows activations to unexpected stimuli. The two networks have shown distinguishable activation even at resting state conditions (Fox et al., 2006). The CEB network consists of anterior and posterior cerebellum on either hemisphere. It consists of the declive and culmen regions. The CEB network has been shown to coordinate with premotor, prefrontal and posterior parietal areas in the cerebral cortex (Bostan et al., 2013). Most of these networks were also confirmed in the ICA analysis and they will be presented in Section 5.3.

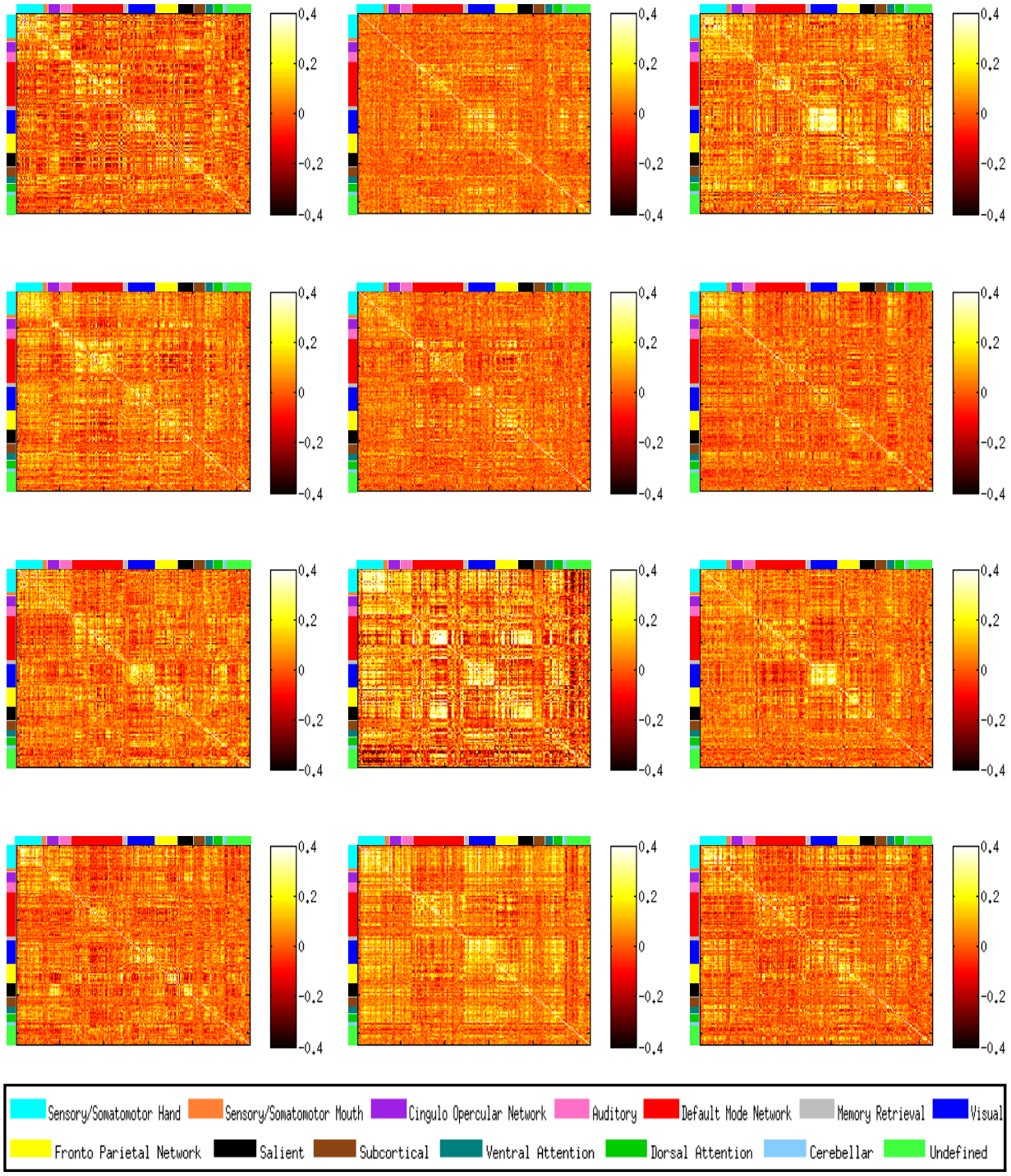

Figure 5.4 Resting State Connectivity for all 12 Subjects from Session 1. All subjects except Subject02 show well defined connectivity in the SM and DMN, V and FPN networks. Subjects 03, 08 and 09 show the strongest correlation in the visual network.

5.2.2 Connectivity Maps After Across Session Regression for INSCAPE

Figure 5.2 shows the subject level functional connectivity of INSCAPE dataset after secondary regression across session. The organization of Figure 5.2 is identical to Figure 5.1. Comparing the connectivity matrix of a representative subject, e.g., Subject01 (first map in the 1st row and 1st column) from REST and INSCAPE shows that the SM, DMN, AUD, Visual, FP, DA and VA Networks demonstrate higher correlation in INSCAPE than in Resting State. Also, the connectivity of the Visual-Attention networks for INSCAPE indicates higher correlation than REST. This is expected because low cognitively demanding INSCAPE can still demand more cognition and attention from brain regions than during REST. Besides, INSCAPE consists of changing 3D digital shapes which will activate the visual-attention network to a higher extent than rest where the subject is just looking at a fixed dot or cross. This could also arise from the dynamic properties of the INSCAPE task. The connectivity map is composed of this property as well and a linear regression may not have any effect on it. The INSCAPE dataset connectivity after secondary regression between subjects show no significant differences compared to this section and therefore not presented here. Subjects 01 and 03 show the strongest correlation in the Visual Network among the 12 subjects. Subject05 shows strong correlations in the DMN and FPN. The inter-network connectivity between DMN and FPN and DMN and DA-VA networks show strong correlation in Subject05.

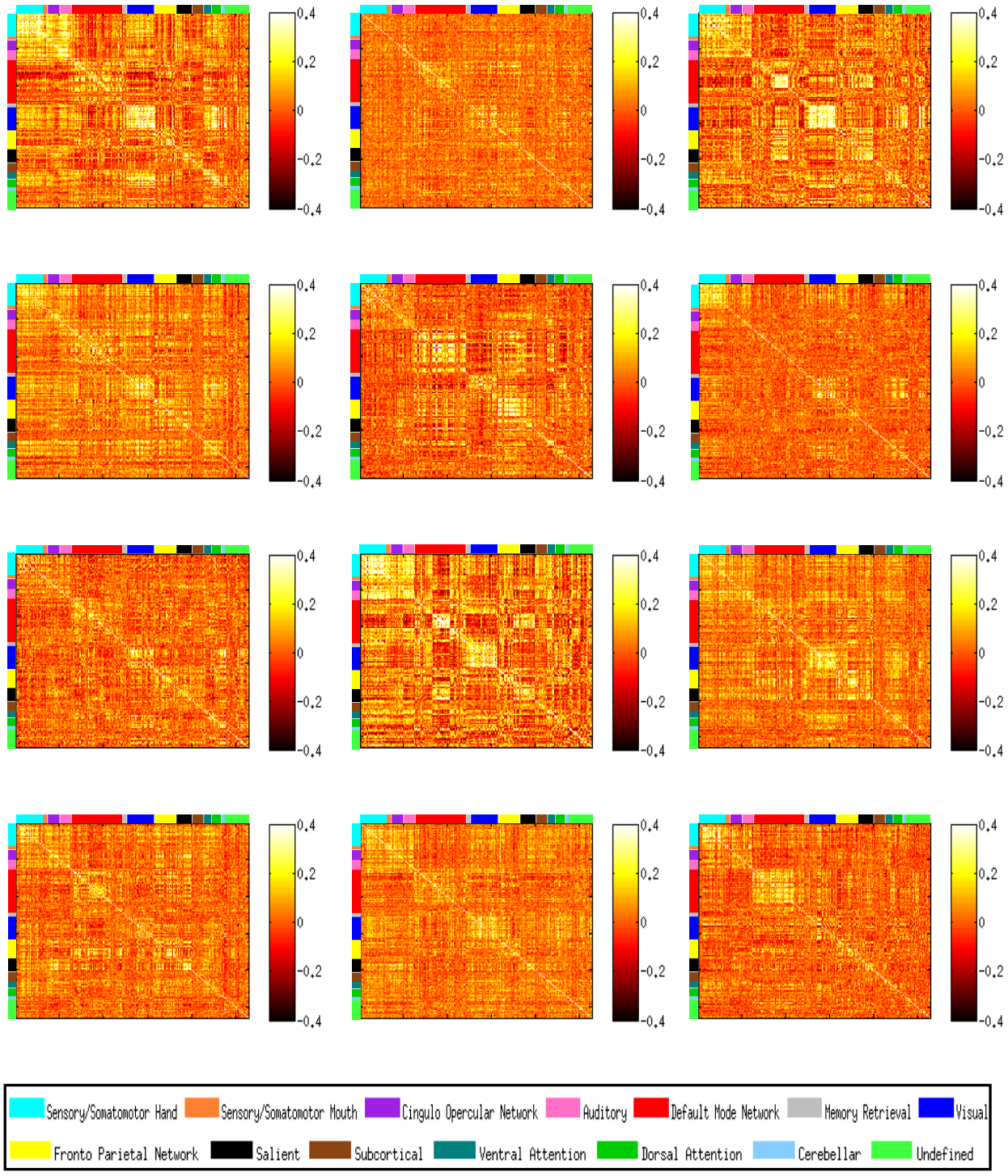

Figure 5.5 Functional Connectivity for INSCAPES after regression of each subject from Session 1 (n=12) across sessions. Subjects 01 and 03 show the strongest correlation in the Visual Network. Subject05 shows strong correlations in the DMN and FPN and inter-connected networks like DMN-FPN and DMN-DA and DMN-VA networks.

5.2.3 Connectivity Maps After Across Session Regression for MOVIE

Figure 5.3 shows the connectivity maps for the MOVIE dataset after secondary regression across sessions. Comparing the connectivity map of a representative subject, e.g., Subject01 (first map in the 1st row and 1st column) from REST and MOVIE after secondary regression across session indicates that the SM, DMN, AUD, Visual, FP, DA and VA networks demonstrates higher correlation in MOVIE than in Resting State. Besides, the Visual, Dorsal and Ventral Attention networks show stronger correlations in MOVIE than the INSCAPE dataset. Also the inter-connectivity of the Visual-Attention networks for MOVIE shows stronger correlation than REST and INSCAPE. This is expected because the MOVIE induces higher cognitive load on the brain regions than either of the other conditions (REST and INSCAPE). This could also arise from the dynamic properties of the MOVIE task which is another part that comprises the functional connectivity and performing a linear regression may not be enough to diminish its effect. The DA and VA networks show the strongest correlations in most subjects compared to REST and INSCAPE. Subjects 01, 03 and 08 show strongest correlation in the Visual network. Strong correlations in inter-network connectivity like DM-SAL, V-DA and V-VA suggest the contribution of these networks for high cognitive demands and attention seeking tasks like MOVIE. MOVIE dataset after secondary regression between subjects do not show any significant differences and therefore not presented here.

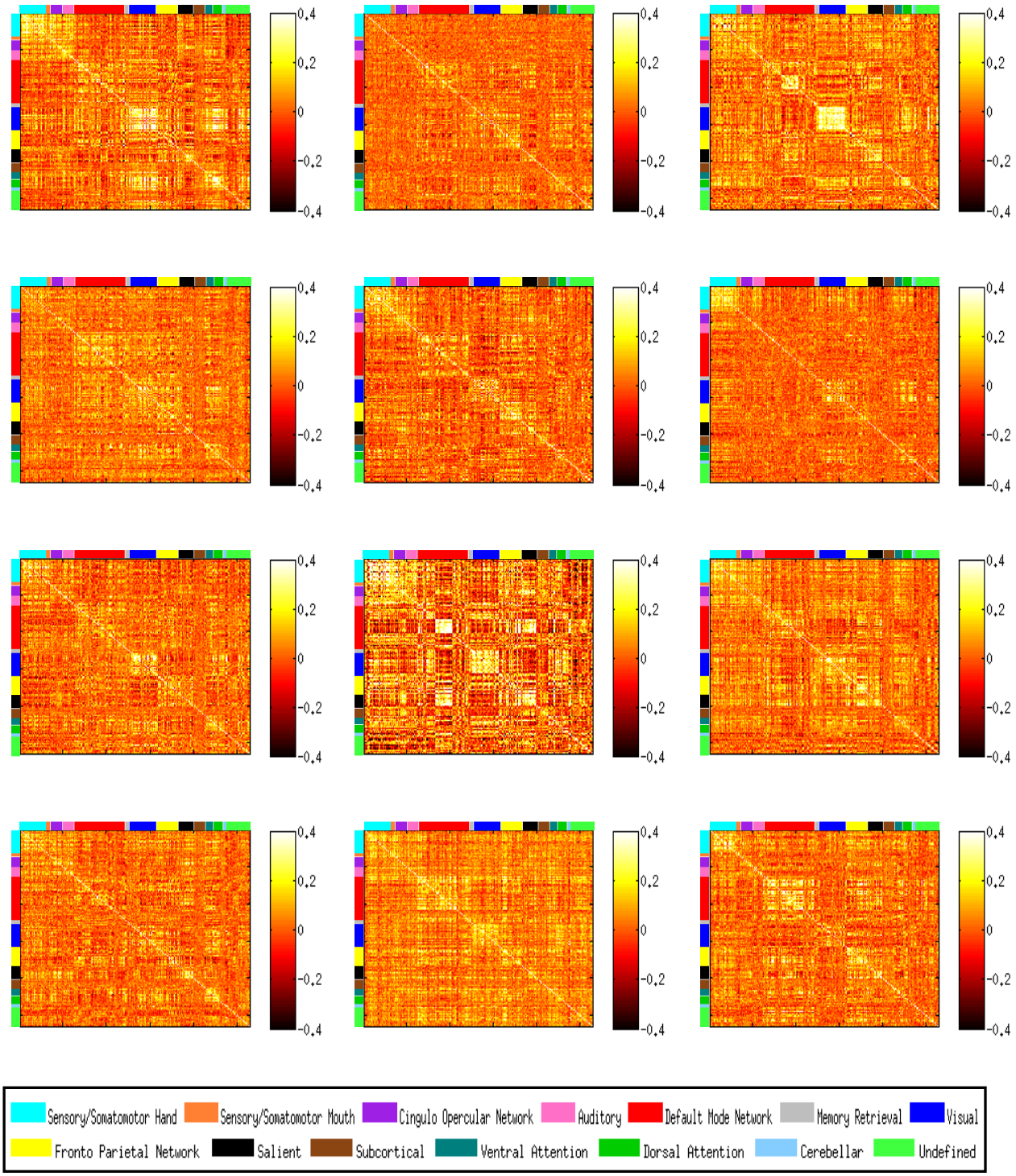

Figure 5.6 Functional Connectivity for MOVIE after regression of each subject from Session 1 (n=12) across sessions. Subjects 01, 03 and 08 show strongest correlation in the Visual (V) network. Majority of Subjects show relatively stronger correlation in the DA and VA networks. Strong Inter-network connectivity between DM-SAL, V-DA and V-VA corresponds to high cognition and attention demands for MOVIE task.

5.3 Group Level Mean Connectivity Maps

In this section, the group level mean connectivity maps is presented. The mean connectivity maps were generated from the average of all the twelve individual connectivity matrices for each condition in Session1. The figure properties are slightly different in this section and the following sub-sections. The legend for the color code of networks is on the right of the connectivity map. The color code for the Fisher's Z transformed correlation values is the same as the previous sections. The range of values is -0.25 to 0.25. The mean connectivity maps show a more defined connectivity of all the major networks.

5.3.1 Mean Functional Connectivity of Rest

Figure 5.4 shows the mean connectivity of REST without performing any secondary regression. The group level measures have a more robust connectivity of SM, AUD, DMN, V, FPN, SAL, DA and VA networks. Note the low correlation in the CO network in REST connectivity. It was mentioned in Section 5.1.1 that this network contributes in tonic alertness. During REST the subjects were instructed to keep eyes open and keep it fixed to a cross on the screen. It is thus likely that this region did not become active during REST. The SMH and Visual networks show the strongest correlation. The inter-network connectivity of DMN-SAL, V-VA and V-DA networks show the lowest correlation among all three conditions. The correlation within VA and DA networks during REST was low compared to INSCAPE and MOVIE. REST was the least cognitively demanding condition.

5.3.2 Mean Functional Connectivity Maps Across Session For Inscapes

Figure 5.5 shows the mean connectivity of INSCAPE dataset after secondary regression across sessions. No significant differences were found from the mean connectivity of the three conditions. The connectivity map of INSCAPE dataset after secondary regression between subjects does not show significant differences. Therefore it is not presented here. The CO network for INSCAPE demonstrated stronger correlation than the REST dataset. The advent of the INSCAPE task would be preceded by the disappearance of a cross. The task has moving and changing shapes that require tonic alertness. It could contribute to higher correlation values in the CO network. Also, the SM and Visual networks show stronger correlations compared to the REST dataset.

5.3.3 Mean Functional Connectivity Maps Across Session For Movie

Figure 5.6 shows the mean connectivity of MOVIE dataset after secondary regression across sessions. The connectivity between the DMN-SAL and V-VA and V-DA networks shows the highest correlation among all three conditions. These networks are associated with cognition, attention, social and emotional paradigms. The connectivity within FPN, SAL, VA and DA networks also demonstrate higher correlation compared to INSCAPE and REST.

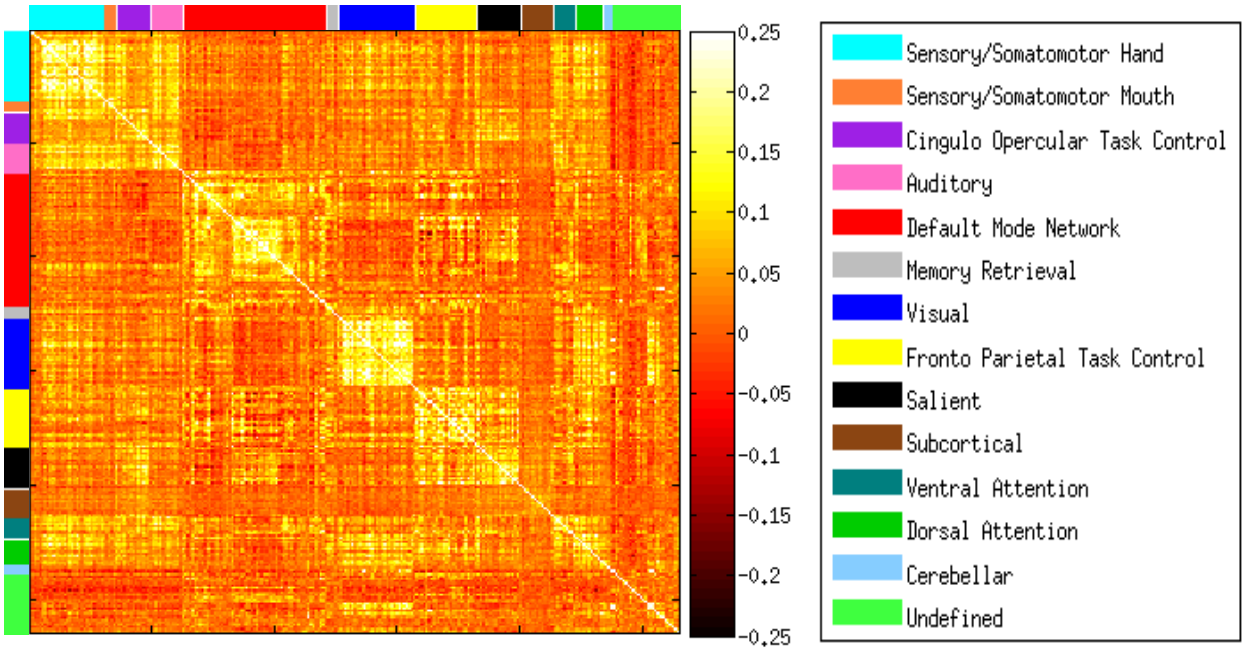

Figure 5.7 Mean Resting State Connectivity of all subjects in Session 1. All major networks show a more rigid structure at the group level. The REST connectivity has the least correlation in DMN-SAL, V-VA and V-DA networks.

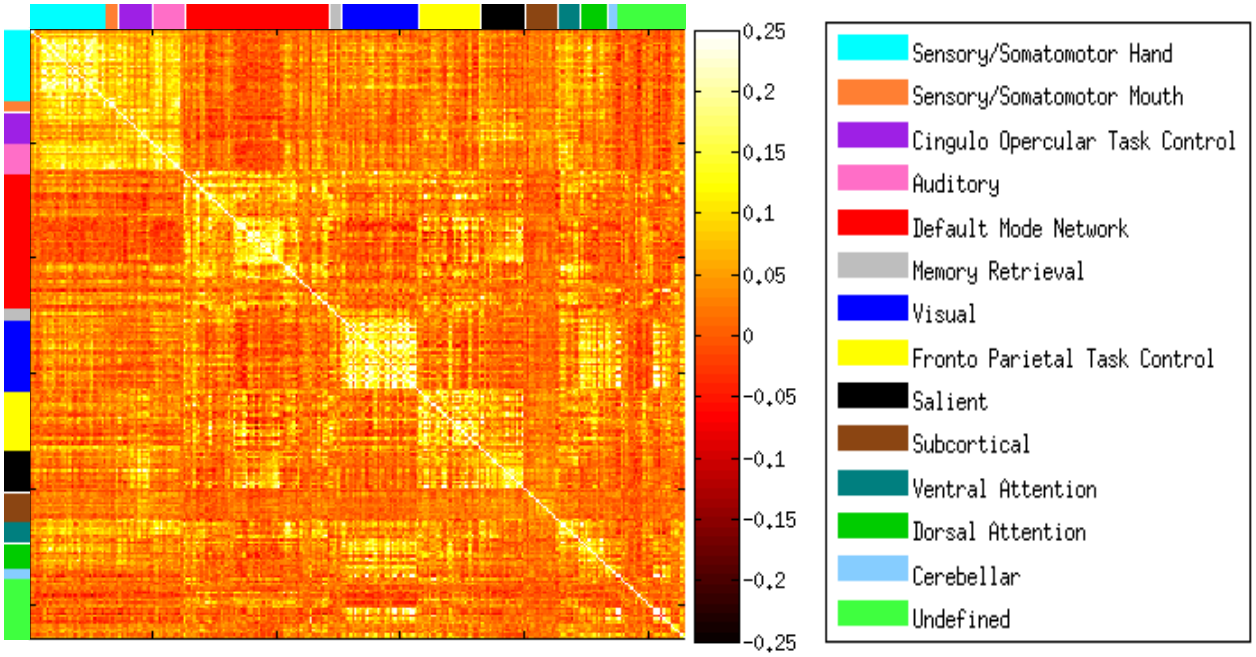

Figure 5.8 Mean Connectivity for INSCAPES after regression of all subjects of Session 1 across all 12 Sessions. Strong correlation found in CON and Visual networks. Lower correlation found in the connectivity regions between networks contributing to higher demand of cognition and attention.

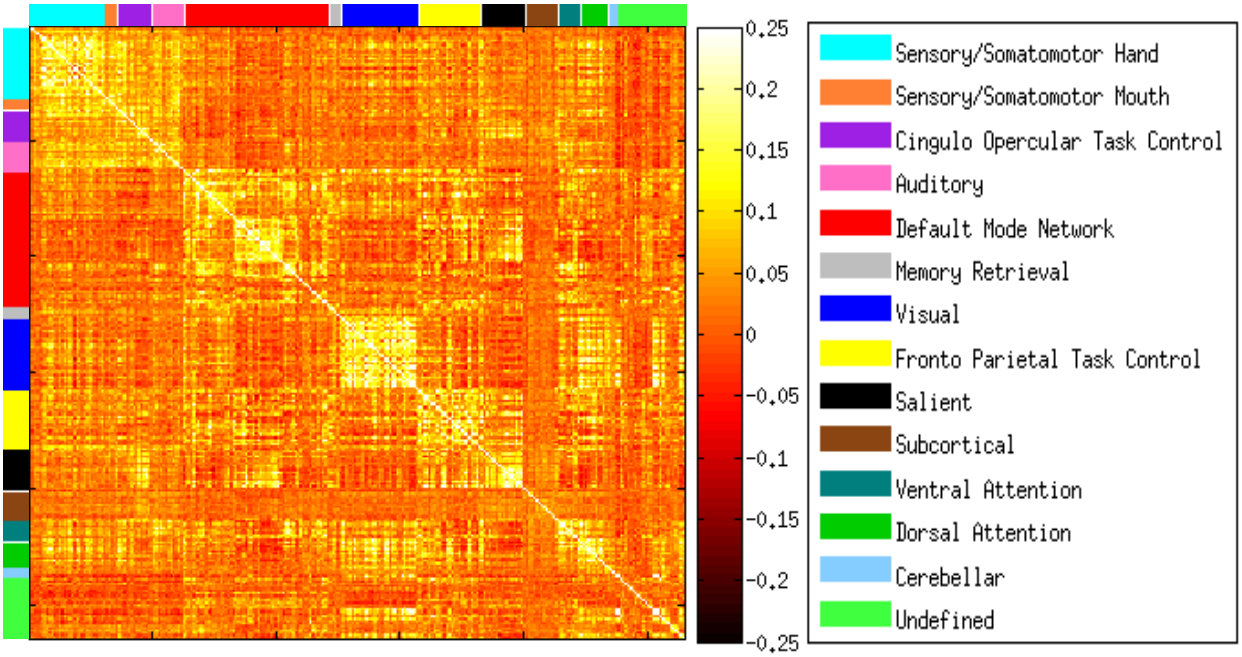

Figure 5.9 Mean Connectivity for MOVIE after regression of all subjects of Session 1 across all 12 Sessions. Strongest correlation found in the DMN-SAL and V-VA and V-DA networks. Highest correlation found in FPN and SAL networks.

5.4 Group Level Paired *t* – test

A group level paired *t* – test was performed on the four condition pairs - INSCAPE vs. REST after secondary regression across sessions and between subjects and similarly for MOVIE vs. REST respectively. The FDR corrected thresholds were accounted for multiple comparisons. An arbitrary p-value threshold of $p < 0.0005$ was considered to show ROI level differences between INSCAPES and MOVIE compared to REST.

5.4.1 Inscapes After Secondary Regression Across Session vs. Rest

Figure 5.10 shows the ROI level significant differences between INSCAPE after secondary regression across sessions and Rest. Thirty Five ROIs showed significant

differences. The horizontal axis shows the ROI pairs and the vertical axis shows the Fisher's Z transformed Mean Correlation values of INSCAPES and REST for each ROI pair. The blue bars are for INSCAPES and the red bars are for REST. Each bar also has a standard error of mean bar associated with it. The black bars with caps on top of each bar represent the error bars. The FDR corrected ROI pair is presented with an asterisk on top for a FDR corrected threshold of $p < 1.1003e\text{-}6$. The full names of ROI pairs in the order they appear on the graph from top to bottom are present in the Appendix, Table A.1. Of all the condition pairs in Table 3.1 this pair has the least number of significant ROI differences with REST.

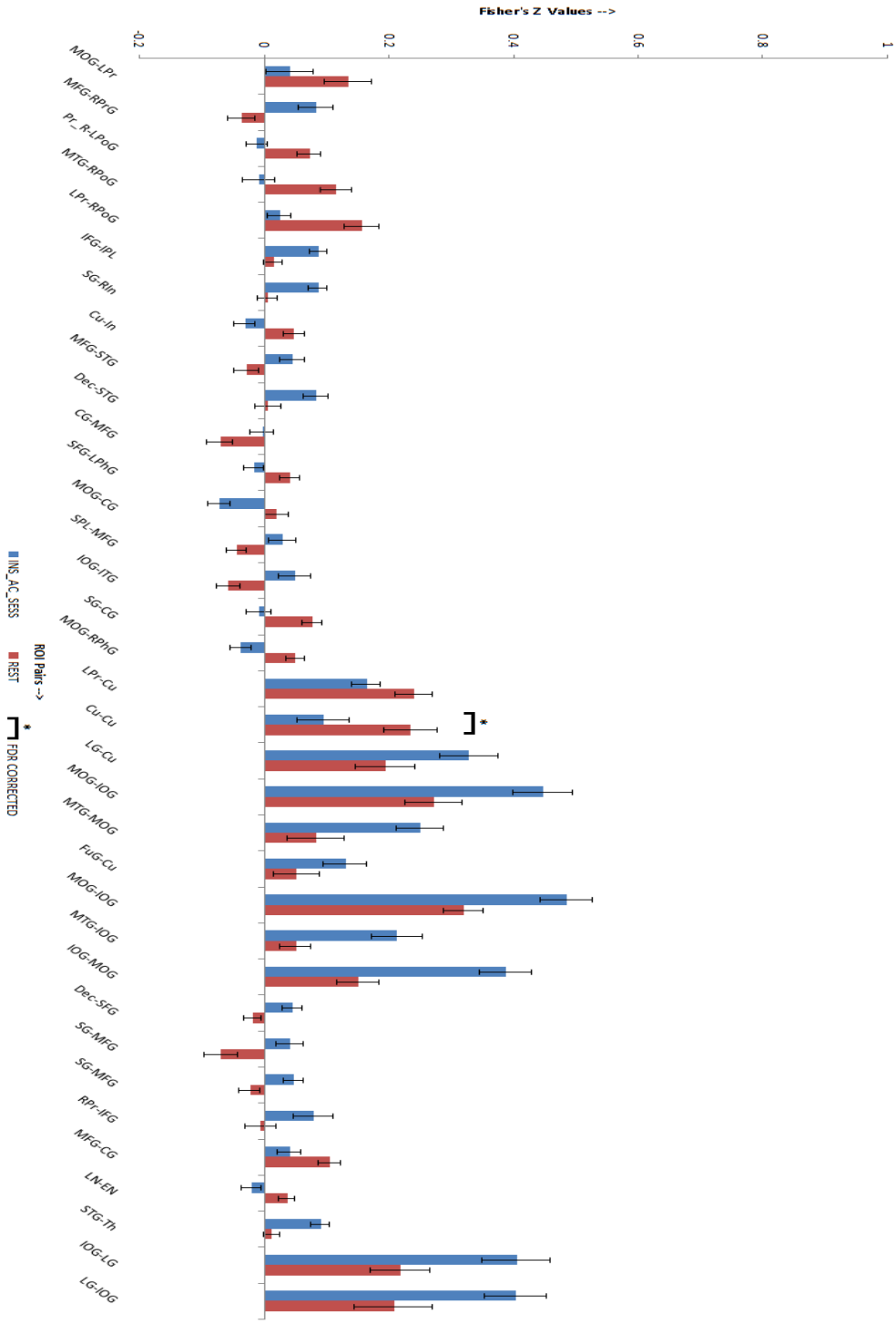

Figure 5.10 Bar Chart showing significant differences in 35 ROI-pairs after conducting a paired *t*-test between INSCAPES after secondary regression across session and REST at an arbitrary p-value threshold of $p < 0.0005$. The chart also shows the Standard Error of Mean (SEM) values as error bars for both INSCAPES and REST. After FDR Correction at $p < 1.1003e\text{-}6$ only one ROI survived shown with a bar and an asterisk (*****) on top.

5.4.2 Inscapes After Secondary Regression Between Subjects vs. Rest

Figure 5.11 shows the ROI level significant differences between INSCAPE after secondary regression between subjects and Rest. Forty one ROIs showed significant differences. The horizontal axis shows the ROI pairs and the vertical axis shows the Fisher's Z transformed Mean Correlation values of INSCAPES and REST for each ROI pair. The blue bars are for INSCAPES and the red bars are for REST. Each bar also has a standard error of mean bar associated with it. The black bars with caps on top of each bar represent the error bars. The FDR corrected ROI pair is presented with an asterisk on top for a FDR corrected threshold of $p < 7.7100e-7$. The full names of ROI pairs in the order they appear on the graph from top to bottom are present in the Appendix, Table A.2. The number of ROIs for INSCAPE after secondary regression between subjects is six more than INSCAPE after secondary regression across sessions.

5.4.3 Movie After Secondary Regression Across Session vs. Rest

Figure 5.12 shows the ROI level significant differences between MOVIE after secondary regression across sessions and Rest. Sixty one ROIs showed significant differences. The horizontal axis shows the ROI pairs and the vertical axis shows the Fisher's Z transformed Mean Correlation values of MOVIE and REST for each ROI pair. The blue bars are for MOVIE and the red bars are for REST. Each bar also has a standard error of mean bar associated with it. The black bars with caps on top of each bar represent the error bars. The FDR corrected ROI pair is presented with an asterisk on top for a FDR corrected threshold of $p < 6.8506e-7$.

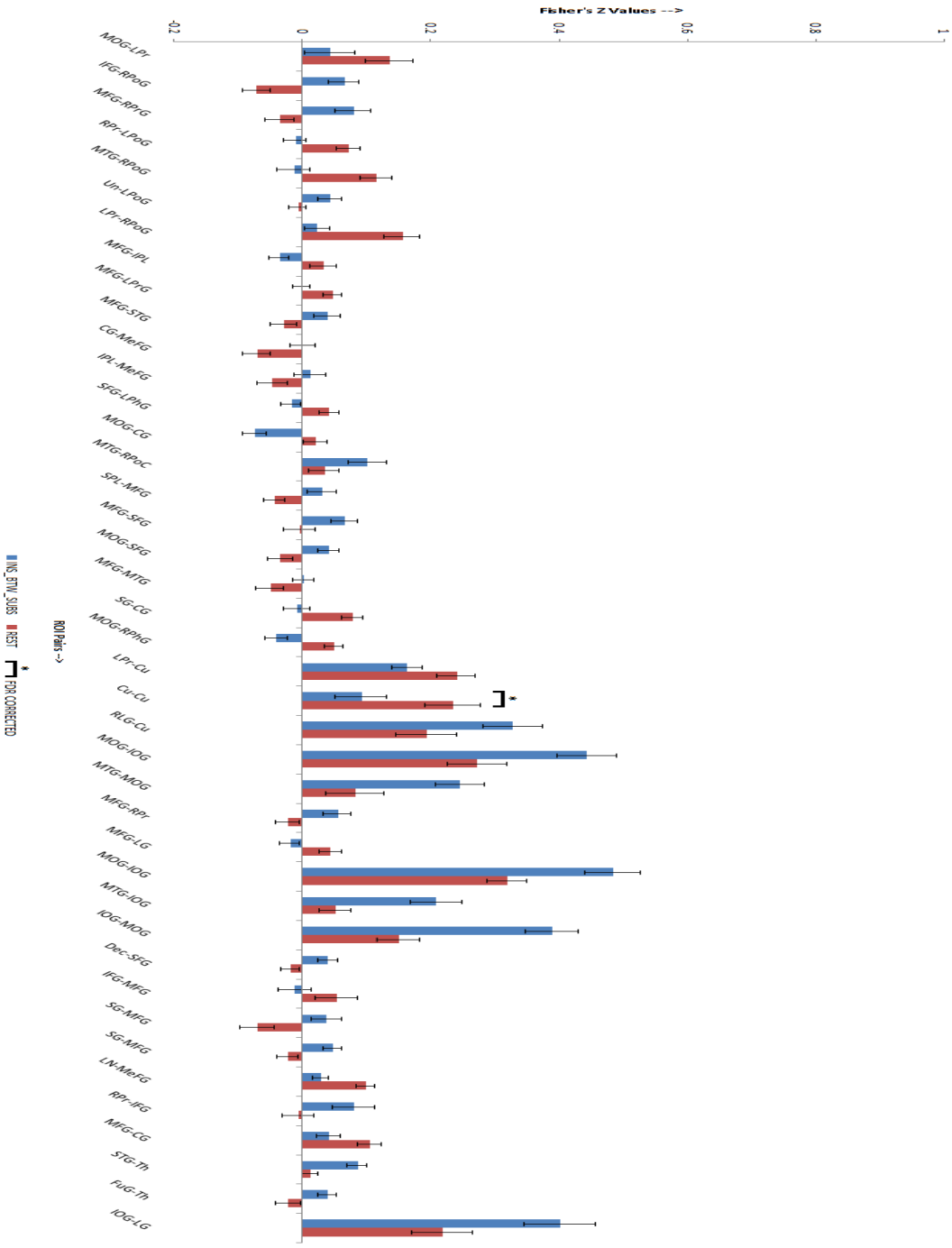

Figure 5.11 Bar Chart showing significant differences in 41 ROI-pairs after conducting a paired *t* – test between INSCAPES after secondary regression between subjects and REST at an arbitrary p-value threshold of $p < 0.0005$. The chart also shows the Standard Error of Mean (SEM) values as error bars for both INSCAPES and REST. After FDR Correction at $p < 7.7100e\text{-}7$ only one ROI survived shown with a bar and an asterisk (*****) on top.

The full names of ROI pairs in the order they appear on the graph from top to bottom are present in the Appendix, Table A.3. The MOVIE dataset demonstrated almost a 50% increase in the number of ROIs with significant differences compared to INSCAPE after across session regression.

5.4.4 Movie After Secondary Regression Between Subjects vs. Rest

Figure 5.13 shows the ROI level significant differences between MOVIE after secondary regression between subjects and Rest. Seventy three ROIs showed significant differences. The figure organization is the same as the previous section so they are not repeated here. The full names of ROI pairs in the order they appear on the graph from top to bottom are present in Appendix, Table A.4. This dataset has the highest number of ROIs with significant differences among the four condition pairs mentioned in Section 5.4.

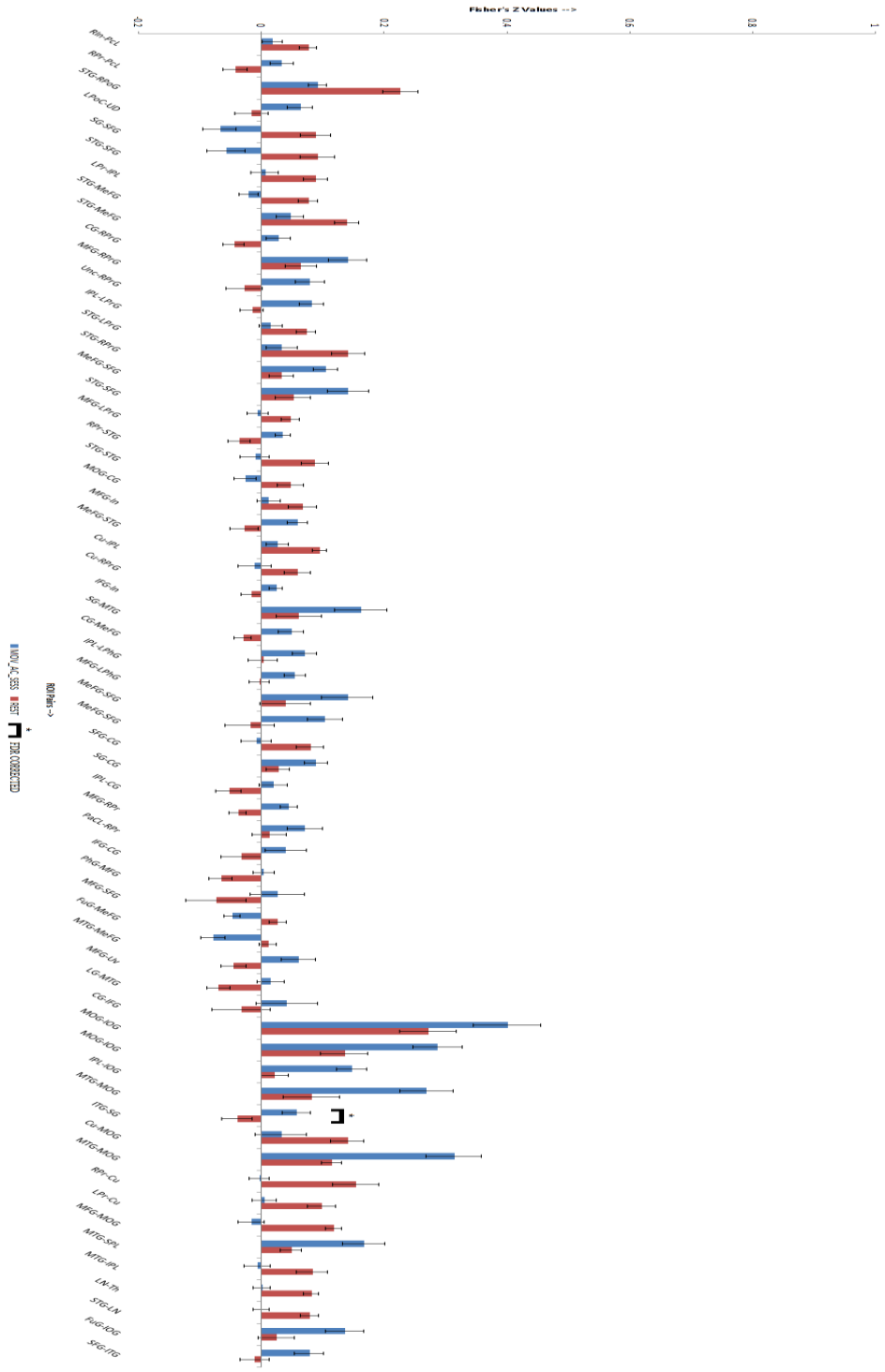

Figure 5.12 Bar Chart showing significant differences in 61 ROI-pairs after conducting a paired *t*-test between MOVIE after secondary regression across session and REST at an arbitrary p-value threshold of $p < 0.0005$. The chart also shows the Standard Error of Mean (SEM) values as error bars for both MOVIE and REST. After FDR Correction at $p < 6.8506e\text{-}7$ only one ROI survived shown with a bar and an asterisk (*****) on top.

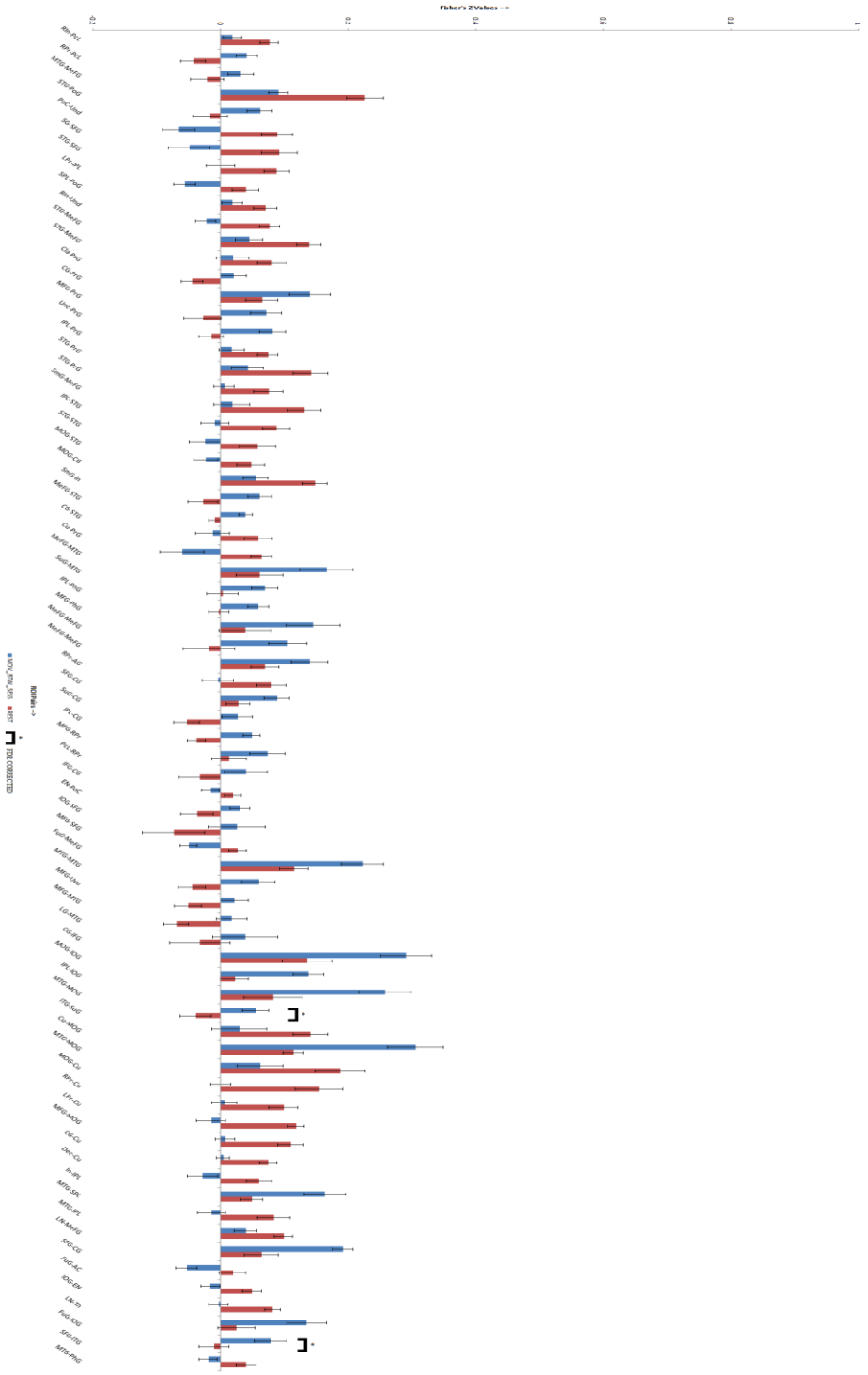

Figure 5.13 Bar Chart showing significant differences in 73 ROI-pairs after conducting a paired *t*-test between MOVIE after secondary regression between subjects and REST at an arbitrary p-value threshold of $p < 0.0005$. The chart also shows the Standard Error of Mean (SEM) values as error bars for both MOVIE and REST. After FDR Correction at $p < 0$ only two ROI survived shown with a bar and an asterisk (*****) on top.

CHAPTER 6

CONCLUSION AND DISCUSSION

6.1 Conclusion

The ICA components demonstrated INSCAPE connectivity is more reliable with higher number of networks for both concatenated and tensor ICA at a limit of 50 components. However, if more components were allowed probably more networks associated with the movie dataset would be generated.

Changes in Functional Connectivity on both individual and group level are considerably lower in INSCAPEs than the conventional MOVIE featured in the current study. The Resting State functional connectivity was taken as the reference base to which both the task conditions were compared. The results of *t* – test and FDR correction show comparatively fewer number of ROIs with significant differences in INSCAPES for both secondary regression methods. Till now, INSCAPE is the only context-less, abstract movie that has been used as an intermediary stage between REST and the traditional MOVIE condition for better head motion compliance in children and adults (Vanderwal et al., 2015). Yet, it is by no means a replacement or alternative to the Resting State paradigm. It can act as a mediating buffer stage between a 'low cognition' (REST) to a 'high cognition' (MOVIE) task. Eventually, studies with more datasets over tuned age population and common movie segments would probably demonstrate more reliable results and converge towards a rigid conclusion. Significant differences in ROIs during both INSCAPE and MOVIE demonstrate fewer differences with REST, after secondary regression across sessions compared to the secondary regression between subjects. It may

be because the subject got acclimatized to both the tasks after performing a few sessions and demanded less cognition and attention. It could be argued that the same may have happened for all subjects in the group. However, each subject's variability may be different than the other subjects. Thus, at the group level, performing a regression between subjects, demonstrate more differences for both the tasks.

Initially, regression was assumed to take out the entire effect of task from each voxel. Practically, the functional connectivity from the task conditions also comprise of dynamic properties from the tasks. However, resting state can be considered just another arbitrary task with the least demand for cognition (Buckner RL et al., 2013). This means, the connectivity is also modified partially from the dynamic properties of the tasks. If this property is reduced, the functional connectivity of INSCAPE could approximate the resting state connectivity. They may not be reduced by a simple linear regression model. An algorithm to reduce specific dynamic properties is required to make a stronger estimation. It could be a future work that is entailed with this study.

The tasks in this study were not typical block design fMRI tasks. They were continuous and dynamic in nature. Thus the level of cognition and attention may have varied non-linearly during the entire task for each subject. Block design studies are helpful in such cases because the timing of the tasks are coherent and easily located. Without block designs, it is difficult to find common temporal variability in subjects over multiple sessions. Thus, instead of investigating specific time points, the overall effect of task was measured in this study. In future, sharp turn of events in the movie segments could be located and functional connectivity could be compared with INSCAPE at those time points. INSCAPES are independent of such sharp changes of content and frame

angles and may serve as a reference to all movies with high cognition demands and social interactions.

6.2 Discussion

This study was based on the work of Dr. Tamara Vanderwal et al. where they improve head motion compliance using INSCAPE and MOVIE. The same naturalistic viewing paradigm was used to investigate functional connectivity changes. MOVIE and INSCAPE evoke spatiotemporal responses in various networks. More spatial Networks are generated from INSCAPE and MOVIE than REST condition within the 50 components limit. This shows more networks are activated during natural viewing paradigms (Uri Hasson et al., 2004 and Vanderwal et al., 2015).

Functional Connectivity is similar across all conditions (Vanderwal et al., 2015, Moeller et al., 2009; Betti et al., 2013). Significant Differences in Sensory Motor, Visual and Visual attention networks for INSCAPE are consistent with results from exisiting studies (Vanderwal et al., 2015). MOVIEs demonstrating highest differences in the Fronto Parietal, Default Mode, Attention, Visual Attention, Salience networks are also consistent with current studies using natural viewing paradigm (Vanderwal et al., 2015). Comparatively, lower differences in INSCAPE indicates Functional Connectivity of INSCAPE is closer to REST condition than conventional MOVIEs.

APPENDIX A

LIST OF ROI PAIR NAMES FROM PAIRED *t* – TEST RESULTS

Tables A.1, A.2, A.3 and A.4 lists the ROI pair names of each condition pair in Table 4.1.

Table A.1 Inscapes After Secondary Regression Across Session vs. Rest

Order No.	Abbreviation	ROI Pair Names
1	MOG-LPr	Middle Occipital Gyrus - Left Precuneus
2	MFG-RPrG	Middle Frontal Gyrus - Right Precentral Gyrus
3	Pr_R-LPoG	Right Precuneus - Left Postcentral Gyrus
4	MTG-RPoG	Middle Temporal Gyrus - Right Postcentral Gyrus
5	LPr-RPoG	Left Precuneus - Right Postcentral Gyrus
6	IFG-IPL	Inferior Frontal Gyrus - Inferior Parietal Lobule
7	SG-RIn	Sub-Gyral - Right Insula
8	Cu-In	Cuneus - Insula
9	MFG-STG	Middle Frontal Gyrus - Superior Temporal Gyrus
10	Dec-STG	Declive - Superior Temporal Gyrus
11	CG-MFG	Cingulate Gyrus - Middle Frontal Gyrus
12	SFG-LPhG	Superior Frontal Gyrus - Left Parahippocampal Gyrus
13	MOG-CG	Middle Occipital Gyrus - Cingulate Gyrus
14	SPL-MFG	Superior Parietal Lobule - Middle Frontal Gyrus
15	IOG-ITG	Inferior Occipital Gyrus - Inferior Temporal Gyrus
16	SG-CG	Sub-Gyral - Cingulate Gyrus
17	MOG-RPhG	Middle Occipital Gyrus - Right Parahippocampal Gyrus
18	LPr-Cu	Left Precuneus - Cuneus
19	Cu-Cu	Cuneus - Cuneus
20	LG-Cu	Lingual Gyrus - Cuneus

Table A.1 Inscapes After Secondary Regression Across Session vs. Rest (Continued)

Order No.	Abbreviation	ROI Pair Names
21	MOG-IOG	Middle Occipital Gyrus - Inferior Occipital Gyrus
22	MTG-MOG	Middle Temporal Gyrus - Middle Occipital Gyrus
23	FuG-Cu	Fusiform Gyrus - Cuneus
24	MOG-IOG	Middle Occipital Gyrus - Inferior Occipital Gyrus
25	MTG-IOG	Middle Temporal Gyrus - Inferior Occipital Gyrus
26	IOG-MOG	Inferior Occipital Gyrus - Middle Occipital Gyrus
27	Dec-SFG	Declive - Superior Frontal Gyrus
28	SG-MFG	Sub-Gyral - Middle Frontal Gyrus
29	SG-MFG	Sub-Gyral - Middle Frontal Gyrus
30	RPr-IFG	Right Precuneus - Inferior Frontal Gyrus
31	MFG-CG	Middle Frontal Gyrus - Cingulate Gyrus
32	LN-EN	Lentiform Nucleus - Extra Nuclear
33	STG-Th	Superior Temporal Gyrus - Thalamus
34	IOG-LG	Inferior Occipital Gyrus - Lingual Gyrus
35	LG-IOG	Lingual Gyrus - Inferior Occipital Gyrus

Table A.2 Inscapes After Secondary Regression Between Subjects vs. Rest

Order No.	Abbreviation	ROI Pair Names
1	MOG-LPr	Middle Occipital Gyrus - Left Precuneus
2	IFG-RPoG	Inferior Frontal Gyrus - Right Postcentral Gyrus
3	MFG-RPrG	Middle Frontal Gyrus - Right Precentral Gyrus
4	RPr-LPoG	Right Precuneus - Left Postcentral Gyrus
5	MTG-RPoG	Middle Temporal Gyrus - Right Postcentral Gyus
6	Un-LPoG	Uncus - Left Postcentral Gyrus

Table A.2 Inscapes After Secondary Regression Between Subjects vs. Rest (Continued)

Order No.	Abbreviation	ROI Pair Names
7	LPr-RPoG	Left Precuneus - Right Postcentral Gyrus
8	MFG-IPL	Middle Frontal Gyrus - Inferior Parietal Lobule
9	MFG-LPrG	Middle Frontal Gyrus - Left Precentral Gyrus
10	MFG-STG	Middle Frontal Gyrus - Superior Temporal Gyrus
11	CG-MeFG	Cingulate Gyrus - Medial Frontal Gyrus
12	IPL-MeFG	Inferior Parietal Lobule - Medial Frontal Gyrus
13	SFG-LPhG	Superior Frontal Gyrus - Left Parahippocampal Gyrus
14	MOG-CG	Middle Occipital Gyrus - Cingulate Gyrus
15	MTG-RPoC	Middle Temporal Gyrus - Right Postcentral Gyrus
16	SPL-MFG	Superior Parietal Lobule - Middle Frontal Gyrus
17	MFG-SFG	Middle Frontal Gyrus - Superior Frontal Gyrus
18	MOG-SFG	Middle Occipital Gyrus - Superior Frontal Gyrus
19	MFG-MTG	Middle Frontal Gyrus - Middle Temporal Gyrus
20	SG-CG	Sub-Gyral - Cingulate Gyrus
21	MOG-RPhG	Middle Occipital Gyrus - Right Parahippocampal Gyrus
22	LPr-Cu	Left Precuneus - Cuneus
23	Cu-Cu	Cuneus - Cuneus
24	RLG-Cu	Right Lingual Gyrus - Cuneus
25	MOG-IOG	Middle Occipital Gyrus - Inferior Occipital Gyrus
26	MTG-MOG	Middle Temporal Gyrus - Middle Occipital Gyrus
27	MFG-RPr	Middle Frontal Gyrus - Right Precuneus
28	MFG-LG	Middle Frontal Gyrus - Lingual Gyrus
29	MOG-IOG	Middle Occipital Gyrus - Inferior Occipital Gyrus
30	MTG-IOG	Middle Temporal Gyrus - Inferior Occipital Gyrus
31	IOG-MOG	Inferior Occipital Gyrus - Middle Occipital Gyrus

Table A.2 Inscapes After Secondary Regression Between Subjects vs. Rest (Continued)

Order No.	Abbreviation	ROI Pair Names
32	Dec-SFG	Declive - Superior Frontal Gyrus
33	IFG-MFG	Inferior Frontal Gyrus - Middle Frontal Gyrus
34	SG-MFG	Sub-Gyral - Middle Frontal Gyrus
35	SG-MFG	Sub-Gyral - Middle Frontal Gyrus
36	LN-MeFG	Lentiform Nucleus - Medial Frontal Gyrus
37	RPr-IFG	Right Precuneus - Inferior Frontal Gyrus
38	MFG-CG	Middle Frontal Gyrus - Cingulate Gyrus
39	STG-Th	Superior Temporal Gyrus - Thalamus
40	FuG-Th	Fusiform Gyrus - Thalamus
41	IOG-LG	Inferior Occipital Gyrus - Lingual Gyrus

Table A.3 Movie After Secondary Regression Across Session vs. Rest

Order No.	Abbreviation	ROI Pair Names
1	RIn-PcL	Right Insula - Paracentral Lobule
2	RPr-PcL	Right Precuneus - Paracentral Lobule
3	STG-RPoG	Superior Temporal Gyrus - Right Postcentral Gyrus
4	LPoC-UD	Left Postcentral Gyrus - Undefined
5	SG-SFG	Sub-Gyral - Superior Frontal Gyrus
6	STG-SFG	Superior Temporal Gyrus - Superior Frontal Gyrus
7	LPr-IPL	Left Precuneus - Inferior Parietal Lobule
8	STG-MeFG	Superior Temporal Gyrus - Medial Frontal Gyrus
9	STG-MeFG	Superior Temporal Gyrus - Medial Frontal Gyrus
10	CG-RPrG	Cingulate Gyrus - Right Precentral Gyrus
11	MFG-RPrG	Middle Frontal Gyrus - Right Precentral Gyrus

Table A.3 Movie After Secondary Regression Across Session vs. Rest (Continued)

Order No.	Abbreviation	ROI Pair Names
12	Unc-RPrG	Uncus - Right Precentral Gyrus
13	IPL-LPrG	Inferior Parietal Lobule - Left Precentral Gyrus
14	STG-LPrG	Superior Temporal Gyrus - Left Precentral Gyrus
15	STG-RPrG	Superior Temporal Gyrus - Right Precentral Gyrus
16	MeFG-SFG	Medial Frontal Gyrus - Superior Frontal Gyrus
17	STG-SFG	Superior Temporal Gyrus - Superior Frontal Gyrus
18	MFG-LPrG	Middle Frontal Gyrus - Left Precentral Gyrus
19	RPr-STG	Right Precuneus - Superior Temporal Gyrus
20	STG-STG	Superior Temporal Gyrus - Superior Temporal Gyrus
21	MOG-CG	Middle Occipital Gyrus - Cingulate Gyrus
22	MFG-In	Middle Frontal Gyrus - Insula
23	MeFG-STG	Medial Frontal Gyrus - Superior Temporal Gyrus
24	Cu-IPL	Cuneus - Inferior Parietal Lobule
25	Cu-RPrG	Cuneus - Right Precentral Gyrus
26	IFG-In	Inferior Frontal Gyrus - Insula
27	SG-MTG	Sub-Gyral - Middle Temporal Gyrus
28	CG-MeFG	Cingulate Gyrus - Medial Frontal Gyrus
29	IPL-LPhG	Inferior Parietal Lobule - Left Parahippocampal Gyrus
30	MFG-LPhG	Middle Frontal Gyrus - Left Parahippocampal Gyrus
31	MeFG-SFG	Medial Frontal Gyrus - Superior Frontal Gyrus
32	MeFG-SFG	Medial Frontal Gyrus - Superior Frontal Gyrus
33	SFG-CG	Superior Frontal Gyrus - Cingulate Gyrus
34	SG-CG	Sub-Gyral - Cingulate Gyrus
35	IPL-CG	Inferior Parietal Lobule - Cingulate Gyrus
36	MFG-RPr	Middle Frontal Gyrus - Right Precuneus

Table A.3 Movie After Secondary Regression Across Session vs. Rest (Continued)

Order No.	Abbreviation	ROI Pair Names
37	PaCL-RPr	Paracentral Lobule - Right Precuneus
38	IFG-CG	Inferior Frontal Gyrus - Cingulate Gyrus
39	PhG-MFG	Parahippocampal Gyrus - Middle Frontal Gyrus
40	MFG-SFG	Middle Frontal Gyrus - Superior Frontal Gyrus
41	FuG-MeFG	Fusiform Gyrus - Medial Frontal Gyrus
42	MTG-MeFG	Middle Temporal Gyrus - Medial Frontal Gyrus
43	MFG-Uv	Middle Frontal Gyrus - Uvula
44	LG-MTG	Lingual Gyrus - Middle Temporal Gyrus
45	CG-IFG	Cingulate Gyrus - Inferior Frontal Gyrus
46	MOG-IOG	Middle Occipital Gyrus - Inferior Occipital Gyrus
47	MOG-IOG	Middle Occipital Gyrus - Inferior Occipital Gyrus
48	IPL-IOG	Inferior Parietal Lobule - Inferior Occipital Gyrus
49	MTG-MOG	Middle Temporal Gyrus - Middle Occipital Gyrus
50	ITG-SG	Inferior Temporal Gyrus - Sub-Gyral
51	Cu-MOG	Cuneus - Middle Occipital Gyrus
52	MTG-MOG	Middle Temporal Gyrus - Middle Occipital Gyrus
53	RPr-Cu	Right Precuneus - Cuneus
54	LPr-Cu	Left Precuneus - Cuneus
55	MFG-MOG	Middle Frontal Gyrus - Middle Occipital Gyrus
56	MTG-SPL	Middle Temporal Gyrus - Superior Parietal Lobule
57	MTG-IPL	Middle Temporal Gyrus - Inferior Parietal Lobule
58	LN-Th	Lentiform Nucleus - Thalamus
59	STG-LN	Superior Temporal Gyrus - Lentiform Nucleus
60	FuG-IOG	Fusiform Gyrus - Inferior Occipital Gyrus
61	SFG-ITG	Superior Frontal Gyrus - Inferior Temporal Gyrus

Table A.4 Movie After Secondary Regression Between Subjects vs. Rest

Order No.	Abbreviation	ROI Pair Names
1	RIn-PcL	Right Insula - Paracentral Lobule
2	RPr-PcL	Right Precuneus - Paracentral Lobule
3	MTG-MeFG	Middle Temporal Gyrus - Medial Frontal Gyrus
4	STG-PoG	Superior Temporal Gyrus - Postcentral Gyrus
5	PoC-Und	Postcentral Gyrus - Undefined
6	SG-SFG	Sub-Gyral - Superior Frontal Gyrus
7	STG-SFG	Superior Temporal Gyrus - Superior Frontal Gyrus
8	LPr-IPL	Left Precuneus - Inferior Parietal Lobule
9	SPL-PoG	Superior Parietal Lobule - Postcentral Gyrus
10	RIn-Und	Right Insula - Undefined
11	STG-MeFG	Superior Temporal Gyrus - Medial Frontal Gyrus
12	STG-MeFG	Superior Temporal Gyrus - Medial Frontal Gyrus
13	Cla-PrG	Claustrum - Precentral Gyrus
14	CG-PrG	Cingulate Gyrus - Precentral Gyrus
15	MFG-PrG	Middle Frontal Gyrus - Precentral Gyrus
16	Unc-PrG	Uncus - Precentral Gyrus
17	IPL-PrG	Inferior Parietal Lobule - Precentral Gyrus
18	STG-PrG	Superior Temporal Gyrus - Precentral Gyrus
19	STG-PrG	Superior Temporal Gyrus - Precentral Gyrus
20	SmG-MeFG	Supramarginal Gyrus - Medial Frontal Gyrus
21	IPL-STG	Inferior Parietal Lobule - Superior Temporal Gyrus
22	STG-STG	Superior Temporal Gyrus - Superior Temporal Gyrus
23	MOG-STG	Middle Occipital Gyrus - Superior Temporal Gyrus
24	MOG-CG	Middle Occipital Gyrus - Cingulate Gyrus
25	SmG-In	Supramarginal Gyrus - Insula

Table A.4 Movie After Secondary Regression Between Subjects vs. Rest (Continued)

Order No.	Abbreviation	ROI Pair Names
26	MeFG-STG	Medial Frontal Gyrus - Superior Frontal Gyrus
27	CG-STG	Cingulate Gyrus - Superior Temporal Gyrus
28	Cu-PrG	Cuneus - Precentral Gyrus
29	MeFG-MTG	Medial Frontal Gyrus - Middle Temporal Gyrus
30	SuG-MTG	Sub-Gyral - Middle Temporal Gyrus
31	IPL-PhG	Inferior Parietal Lobule - Parahippocampal Gyrus
32	MFG-PhG	Middle Frontal Gyrus - Parahippocampal Gyrus
33	MeFG-MeFG	Medial Frontal Gyrus - Medial Frontal Gyrus
34	MeFG-MeFG	Medial Frontal Gyrus - Medial Frontal Gyrus
35	RPr-AG	Right Precuneus - Angular Gyrus
36	SFG-CG	Superior Frontal Gyrus - Cingulate Gyrus
37	SuG-CG	Sub-Gyral - Cingulate Gyrus
38	IPL-CG	Inferior Parietal Lobule - Cingulate Gyrus
39	MFG-RPr	Middle Frontal Gyrus - Right Precuneus
40	PcL-RPr	Paracentral Lobule - Right Precuneus
41	IFG-CG	Inferior Frontal Gyrus - Cingulate Gyrus
42	EN-PoC	Extra-Nuclear - Postcentral Gyrus
43	IOG-SFG	Inferior Occipital Gyrus - Superior Frontal Gyrus
44	MFG-SFG	Middle Frontal Gyrus - Superior Frontal Gyrus
45	FuG-MeFG	Fusiform Gyrus - Medial Fusifrom Gyrus
46	MTG-MTG	Middle Temporal Gyrus - Middle Temporal Gyrus
47	MFG-Uvu	Middle Frontal Gyrus - Uvula
48	MFG-MTG	Middle Frontal Gyrus - Middle Temporal Gyrus
49	LG-MTG	Lingual Gyrus - Middle Temporal Gyrus
50	CG-IFG	Cingulate Gyrus - Inferior Frontal Gyrus

Table A.4 Movie After Secondary Regression Between Subjects vs. Rest (Continued)

Order No.	Abbreviation	ROI Pair Names
51	MOG-IOG	Middle Occipital Gyrus - Inferior Occipital Gyrus
52	IPL-IOG	Inferior Parietal Lobule - Inferior Occipital Gyrus
53	MTG-MOG	Middle Temporal Gyrus - Middle Occipital Gyrus
54	ITG-SuG	Inferior Temporal Gyrus - Sub-Gyral
55	Cu-MOG	Cuneus - Middle Occipital Gyrus
56	MTG-MOG	Middle Temporal Gyrus - Middle Occipital Gyrus
57	MOG-Cu	Middle Occipital Gyrus - Cuneus
58	RPr-Cu	Right Precuneus - Cu
59	LPr-Cu	Left Precuneus - Cu
60	MFG-MOG	Middle Frontal Gyrus - Middle Occipital Gyrus
61	CG-Cu	Cingulate Gyrus - Cuneus
62	Dec-Cu	Declive - Cuneus
63	In-IPL	Insula - Inferior Parietal Lobule
64	MTG-SPL	Middle Temporal Gyrus - Superior Parietal Lobule
65	MTG-IPL	Middle Temporal Gyrus - Inferior Parietal Lobule
66	LN-MeFG	Lentiform Nucleus - Medial Frontal Gyrus
67	SFG-CG	Superior Frontal Gyrus - Cingulate Gyrus
68	FuG-AC	Fusiform Gyrus
69	IOG-EN	Inferior Occipital Gyrus - Extra Nuclear
70	LN-Th	Lentiform Nucleus - Thalamus
71	FuG-IOG	Fusiform Gyrus - Inferior Occipital Gyrus
72	SFG-ITG	Superior Frontal Gyrus - Inferior Temporal Gyrus
73	MTG-PhG	Middle Temporal Gyrus - Parahippocampal Gyrus

REFERENCES

Anderson JS, Ferguson MA, Lopez-Larson M, Yurgelun-Todd D. Reproducibility of single-subject functional connectivity measurements. *AJNR American journal of neuroradiology*. 2011; 32:548–555. [PubMed: 21273356]

Andreea C Bostan, Richard P Dum, and Peter L Strick. Cerebellar networks with the cerebral cortex and basal ganglia. *Trends Cogn Sci*. 2013 May; 17(5): 241–254. doi:10.1016/j.tics.2013.03.003.

Beckmann, CF, DeLuca, M, Devlin, JT & Smith, SM Investigations into resting-state connectivity using independent component analysis. Philos. Trans R. Soc. Lond. Biol Sci. 2005. 360, 1001–1013.

Beckmann, CF, Smith SM. Probabilistic independent component analysis for functional magnetic resonance imaging. *IEEE Transactions on Medical Imaging.*Volume: 23, Issue: 2, Feb. 2004; DOI: 10.1109/TMI.2003.822821. [PubMed: 14964560]

Beckmann, CF, Smith S.M.. Tensorial extensions of independent component analysis for multisubject FMRI analysis. *Neuroimage*. 2005 Mar 25; (1):294-311. [PubMed: 15734364]

Betti V, Della Penna S, de Pasquale F, Mantini D, Marzetti L, Romani GL, Corbetta M. Natural scenes viewing alters the dynamics of functional connectivity in the human brain. *Neuron*. 2013; 79:782–797. [PubMed: 23891400]

Birn, RM, Diamond, JB, Smith, MA & Bandettini, PA. Separating respiratory-variation related fluctuations from neuronal-activity-related fluctuations in fMRI. *Neuroimage* 31, 1536–1548 (2006).

Birn RM, Molloy EK, Patriat R, Parker T, Meier TB, Kirk GR, Nair VA, Meyerand ME, Prabhakaran V. The effect of scan length on the reliability of resting-state fMRI connectivity estimates. *Neuroimage*.2013; 83:550–558.

Biswal B, Yetkin FZ, Haughton VM, Hyde JS. Functional connectivity in the motor cortex of resting human brain using echo-planar MRI. *Magnetic resonance in medicine*. 1995; 34:537–541.

Bloch F. Nuclear Induction. *Physical Review* 1946; 70:460-474.

Boynton, GM, Engel, SA, Glover, GH, & Heeger, DJ. 1996. Linear systems analysis of functional magnetic resonance imaging in human V1. *J Neurosci*, **16**(13), 4207–21.

Buckner RL, Krienen FM, Yeo BT. Opportunities and limitations of intrinsic functional connectivity MRI. *Nature Neuroscience*. 2013; 16:832–837. [PubMed: 23799476]

Buckner, RL, Andrews-Hanna, JR, Schacter, DL. "The Brain's Default Network: Anatomy, Function, and Relevance to Disease". *Annals of the New York Academy of Sciences*. 2008; **1124** (1): 1 - 38. *PMID* 18400922. doi:10.1196/annals.1440.011

Sestieri C, Corbetta M, Romani GL, and Shulman GL. Episodic memory retrieval, parietal cortex, and the Default Mode Network: functional and topographic analyses. *J Neurosci*. 2011 March 23; 31(12): 4407–4420. doi:10.1523/JNEUROSCI.3335-10.2011.

Chen S, Ross TJ, Zhan W, et al. Group independent component analysis reveals consistent resting-state networks across multiple sessions. *Brain Res* 2008;1239:141–51

Cho ZH, Ro YM. Reduction of susceptibility artifact in gradient-echo imaging. *Magnetic Resonance in Medicine*. 1992; 23:193. [PubMed: 1734179]

Cohen, MS. Parametric analysis of fMRI data using linear systems methods. *Neuroimage*. 1997; **6**(2), 93–103.

Conroy BR, Singer BD, Guntupalli JS, Ramadge PJ, Haxby JV. Inter-subject alignment of human cortical anatomy using functional connectivity. *Neuroimage*. 2013; 81:400–411. [PubMed: 23685161]

Cordes D. et al., Frequencies contributing to functional connectivity in the cerebral cortex in 'resting-state' data. *Am. J. Neuroradiol*. 2001; 22, 1326–1333.

Cox RW. AFNI: software for analysis and visualization of functional magnetic resonance neuroimages. *Comput Biomed Res*. 1996; 29:162–173.

Craig, AD. How do you feel–now? The anterior insula and human awareness. *Nature Reviews Neuroscience*. 2009; 10, 59–70.

Dale, AM. Optimal experimental design for event-related fMRI. *Human Brain Mapp*, 1999; **8**(2–3), 109–14.

Damasio, Antonio. *The Feeling of What Happens: Body and Emotion in the Making of Consciousness.* 2000; New York: Harcourt.

Friston KJ, Frith CD, Liddle PF, Frackowiak RSJ. Functional connectivity: The principal component analysis of large (PET) data sets. *J Cereb Blood Flow Metab* 1993a; 13:5-14.

Friston, K. Functional and effective connectivity in neuroimaging: A synthesis. *Human Brain Mapping* 1994; **2**, 56–78.

Friston KJ, Williams S, Howard R, Frackowiak RS, Turner R. Movement-related effects in fMRI timeseries. Magnetic Resonance in Medicine. 1996; 35:346–355. [PubMed: 8699946]

Friston, KJ, Fletcher, P, Josephs, O, Holmes, A, Rugg, MD, & Turner, R. Event-related fMRI: Characterizing differential responses. *Neuroimage*, 1998; **7**, 30–40.

Friston KJ, Frith C, Frackowiak RSJ, and Turner R. Characterizing dynamic brain responses with fMRI: A multivariate approach. *Neuroimage*, 1995; 2:166–172.

Fox, MD et al. The human brain is intrinsically organized into dynamic, anti-correlated functional networks. *Proc. Natl Acad. Sci. USA.* 2005; 102, 9673–9678.

Fox MD and Raichle ME. Spontaneous fluctuations in brain activity observed with functional magnetic resonance imaging. *Nature Review Neuroscience.* 2007; 8 700-711

Fox MD, Corbetta M, Snyder AZ, Vincent JL, Raichle ME. Spontaneous neuronal activity distinguishes human dorsal and ventral attention systems. *PNAS.* 2006; 103(26):10046–51.

Glover, GH. Deconvolution of impulse response in event-related BOLD fMRI. *Neuroimage*. 1999; **9**(4), 416–29.

Glover GH. Overview of Functional Magnetic Resonance Imaging. *Neurosurg Clin N Am*. 2011 April; 22(2): 133–139. doi:10.1016/j.nec.2010.11.001.

Greicius M. Resting-state functional connectivity in neuropsychiatric disorders. *Curr Opin Neurol*. 2008; 21:424–430.

Hasson U, Nir Y, Levy I, Fuhrmann G, Malach R. Intersubject synchronization of cortical activity during natural vision. *Science*. 2004; 303:1634–1640. [PubMed: 15016991]

Heeger, David J, and David Ress. "What Does fMRI Tell Us About Neuronal Activity?" *Nature Review Neuroscience.* 2002; 3 (2): 142–51.

Hidalgo-Tabon SS. Theory of gradient coil design methods for magnetic resonance imaging. *Concepts in Magnetic Resonance.* 2010; Part A, Vol. 36A(4) 223–242

Huettel, Scott A, Allen W Song, and Gregory McCarthy. *Functional Magnetic Resonance Imaging.* 2004; Trans. Allen W. Song and Gregory McCarthy. Sunderland, MA: Sinauer.

Hutton C, Bork A, Josephs O, Deichmann R, Ashburner J, Turner R. Image distortion correction in fMRI: A quantitative evaluation. *Neuroimage*. 2002; 16:217–240. [PubMed: 11969330]

Hyvarinen A, Karhunen J and Oja E. Independent Component Analysis. New York. Wiley Interscience Publication. 2001; John Wiley & Sons, Inc.

Jerrold TB, Seibert JA, Leidholdt EMJ, and Boone JM. *The Essential Physics of Medical Imaging.* Philadelphia, Pa: Lippincott Williams & Wilkins, 2012; ISBN: 978-0-7817-8057-5.

Houk JC. Neurophysiology of frontal-subcortical loops. In: Lichter DG, Cummings JL, eds. *Frontal-Subcortical Circuits in Psychiatric and Neurological Disorders*. New York, NY: Guilford Press; 2001; 92-113.

Kim DI, Sui J, Rachakonda S, et al. Identification of Imaging Biomarkers in Schizophrenia: A Coefficient-constrained Independent Component Analysis of the Mind Multi-site Schizophrenia Study. *Neuroinformatics*. 2010 (in press).

Klomp D, Konig W, Hoogduin H et al. Practical design of RF transmit and receive arrays. *Proceedings of European Society of Magnetic Resonance in Medicine and Biology (ESMRMB).* 2011; Congress, Leipzig.

Kwong, KK, Belliveau, JW, Chesler, DA, Goldberg, IE,Weisskoff, RM, Poncelet, BP, Kennedy, DN, Hoppel, BE, Cohen, MS, & Turner, R. Dynamic magnetic resonance imaging of human brain activity during primary sensory stimulation. *Proc Natl Acad Sci U S A*, 1992; **89**(12), 5675–9.

Li SJ, Li Z, Wu G, et al. Alzheimer disease: evaluation of a functional MR imaging index as a marker. *Radiology.*2002; 225:253–259.

Menon, V, & Uddin, LQ. Saliency, switching, attention and control: A network model of insula function. *Brain Structure & Function*. 2010; 214, 655–667.

Moeller S, Nallasamy N, Tsao DY, Freiwald WA. Functional connectivity of the macaque brain across stimulus and arousal states. *The Journal of neuroscience* : *the official journal of the Society for Neuroscience*. 2009; 29:5897–5909. [PubMed: 19420256]

Nguyen VT, Sonkusare S, Stadler J, Hu X, Breakspear M, Guo CC. Distinct Cerebellar Contributions to Cognitive-Perceptual Dynamics During Natural Viewing. *Cerebral Cortex*, 2016; 1-11.

Ogawa, S, Lee, TM, Nayak, A & Glynn, P. *Magnetic Resonance in Medicine*. 1990; 14, 68-78.

Ogawa S, Lee TM, Kay AK and Tank DW. Brain Magnetic Resonance Imaging with Contrast Dependent on Blood Oxygenation. *Proc. Natl. Acad. Sci*. (USA), 1990; 87, 9868-9872

Poldrack RA, Mumford JA, Nichols TE. *Handbook of fMRI data analysis*. 2011; New York, Cambridge University Press.

Posner MI. Orienting of attention. *Q J Exp Psychol.* 1980; 32:3–25

Posner, MI, Petersen, SE, Fox, PT, & Raichle, ME. Localization of cognitive operations in the human brain. *Science*, 1988; **240**(4859), 1627–31.

Power JD, Barnes KA, Snyder AZ, Schlaggar BL, Petersen SE. Spurious but systematic correlations in functional connectivity MRI networks arise from subject motion. *Neuroimage*. 2012; 59:2142–2154. [PubMed: 22019881]

Power JD, Alexander LC, Steven MN, Gagan SW, Kelly AB, Jessica AC et al. Functional network organization of the human brain. *Neuron*. 2011 November 17; 72(4): 665–678. doi:10.1016/j.neuron.2011.09.006.

Raichle, ME and Mintun, MA. Brain work and brain imaging. *Annu. Rev. Neurosci.* 2006; **29**, 449–76.

Sadaghiani S and Mark D. Functional Characterization of the Cingulo-Opercular Network in the Maintenance of Tonic Alertness. *Cerebral Cortex September* 2015;25:2763–2773 doi:10.1093/cercor/bhu072

Seger CA. The basal ganglia in human learning. *Neuroscientist*. 2006; 12:285-290.

Shulman, RG, Rothman, DL, Behar, KL & Hyder, F. Energetic basis of brain activity: implications for neuroimaging. *Trends Neurosci.* 2004; **27**, 489–495.

Smith SM, Fox PT, Miller KL, Glahn DC, P. et al. Correspondence of the brain's functional architecture during activation and rest. *PNAS.* 2009**;** 13040–13045.

Stefano S, Marco B, Marco RG, et al. Weighing brain activity with the balance: Angelo Mosso's original manuscripts come to light. *Brain.* 2014; 137; 621–633.

Vanderwal T et al. Inscapes: a movie paradigm to improve compliance in functional magnetic resonance imaging. *Neuroimage*. 2015 November 15; 122: 222–232. doi:10.1016/j.neuroimage.2015.07.069.

Wang J, Ren Y, Hu X, Nguyen VT, Guo L, Han J, and Guo CC. Test–Retest Reliability of Functional Connectivity Networks During Naturalistic fMRI Paradigms. *Human Brain Mapping* 2017; 38:2226–2241